SANDIA REPORT

SAND87—1787 • UC—62
Unlimited Release
Printed November 1987

The Effect of Asymmetric Heating on Flow Stability and Heat Transfer for Flow in a Vertical Tube

Charles H. Tappan

Prepared by
Sandia National Laboratories
Albuquerque, New Mexico 87185 and Livermore, California 94550
for the United States Department of Energy
under Contract DE-AC04-76DP00789

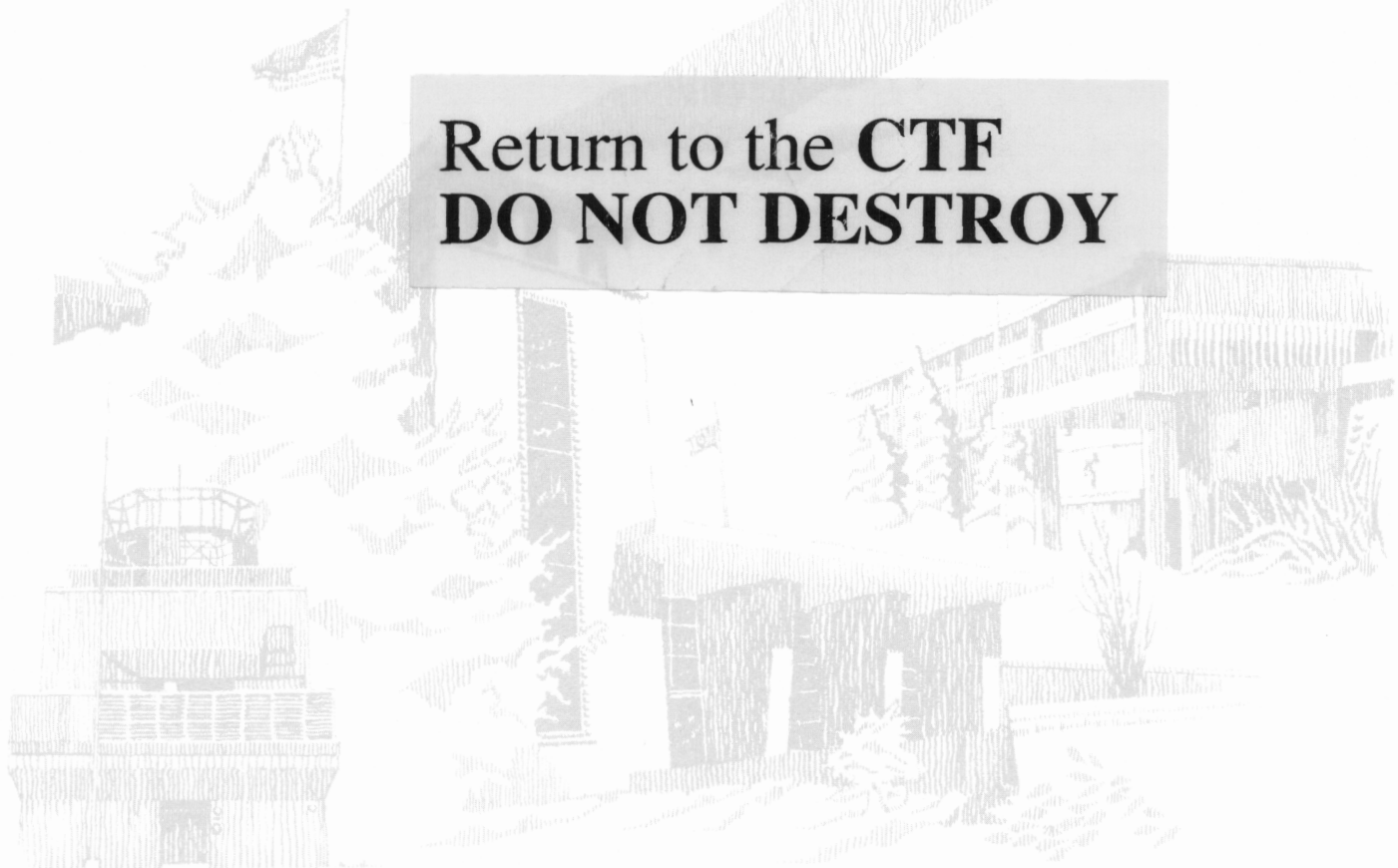

SF2900Q(8-81)

Issued by Sandia National Laboratories, operated for the United States Department of Energy by Sandia Corporation.

Printed in the United States of America
Available from
National Technical Information Service
U.S. Department of Commerce
5285 Port Royal Road
Springfield, VA 22161

NTIS price codes
Printed copy: A04
Microfiche copy: A01

Distribution
Category UC-62

SAND87-1787
Unlimited Release
Printed November 1987

The Effect of Asymmetric Heating on Flow Stability and Heat Transfer for Flow in a Vertical Tube

Charles H. Tappan

Solar Energy Department
Sandia National Laboratories
Albuquerque, New Mexico 87185

ABSTRACT

This study presents experimental results of combined free and forced convection heat transfer in a vertical tube with a circumferentially nonuniform constant wall heat flux. The effect of an asymmetric wall heat flux on flow stability and on the rate of heat transfer for water flowing downward in a vertical tube was investigated. Experimental results were used to develop two stability maps which identify various flow regimes, corresponding to different thermal and hydraulic conditions. Heat transfer coefficients were also determined. Experimental results in the present investigation were compared to those with uniform heating in horizontal and vertical tube flow situations discussed in the literature.

ACKNOWLEDGEMENTS

The author wishes to express his gratitude to Dr. J. R. Leith, Dr. M. W. Wildin, and Dr. W. Gross, of the Department of Mechanical Engineering at the University of New Mexico, and John Otts (6222), John Holmes (6226), Bob Edgar (6222) and Milton Stomp (6222) of Sandia National Laboratories for their experimental support and financial assistance, and for the use of the facilities at the Central Receiver Test Facility at Sandia National Laboratories.

TABLE OF CONTENTS

LIST OF FIGURES

LIST OF TABLES

NOMENCLATURE

A	cross sectional area (m^2)
As	surface area (m^2)
C	degrees Celsius (°C)
D	diameter (m)
Δ	denotes a differential quantity
$\Delta T/\Delta x$	axial bulk fluid temperature gradient (°C/m)
g	gravitational constant (9.81 m/s^2)
L	length (m)
M	mass flowrate, $M = \rho VA$ (kg/s)
p	pressure (Pa)
q	heating power (W)
q'	heating power per unit length (W/m)
q"	heat flux (W/m^2)
R	radius (m)
t	time (s)
T	temperature (°C)
Ti	average fluid inlet temperature (°C)
To	average fluid outlet temperature (°C)
Tb	average bulk fluid temperature (°C)
Tw	average wall temperature (°C)
V	average fluid velocity (m/s)
α	thermal diffusivity (m^2/s)
β	coefficient of thermal expansion (K^{-1})
Cp	specific heat (J/kg°C)
h	heat transfer coefficient (W/m^2°C)
k	thermal conductivity (W/m°C)
ρ	density (kg/m^3)
μ	absolute viscosity (kg/ms)
ν	kinematic viscosity (m^2/s)
f	friction factor
Gr	Grashof number, $Gr = (D^4\rho^2 g\beta q")/(k\alpha^2)$
Nu	Nusselt number, $Nu = (hD)/k$

Pr	Prandtl number, ν/α
Ra	Rayleigh number, $Ra = [g\beta(\Delta T/\Delta x)D^4]/(\nu\alpha)$
Re	Reynolds number, $Re = (\rho VD)/\mu$

FOREWORD

The research and development described in this document was conducted within the U.S. Department of Energy's (DOE) Solar Thermal Technology Program. The goal of the Solar Thermal Technology Program is to advance the engineering and scientific understanding of solar thermal technology, and to establish the technology base from which private industry can develop solar thermal power production options for introduction into the competitive energy market.

Solar thermal technology concentrates solar radiation by means of tracking mirrors or lenses onto a receiver where the solar energy is absorbed as heat and converted into electricity or incorporated into products as process heat. The two primary solar thermal technologies, central receivers and distributed receivers, employ various point and line-focus optics to concentrate sunlight. Current central receiver systems use fields of heliostats (two-axis tracking mirrors) to focus the sun's radiant energy onto a single tower-mounted receiver. Parabolic dishes up to 17 meters in diameter track the sun in two axes and use mirrors to focus radiant energy onto a receiver. Troughs and bowls are line-focus tracking reflectors that concentrate sunlight onto receiver tubes along their focal lines. Concentrating collector modules can be used alone or in a multi-module system. The concentrated radiant energy absorbed by the solar thermal receiver is transported to the conversion process by a circulating working fluid. Receiver temperatures range from 100C in low-temperature troughs to over 1500C in dish and central receiver systems.

The Solar Thermal Technology Program is directing efforts to advance and improve promising system concepts through the research and development of solar thermal materials, components, and subsystems, and the testing and performance evaluation of subsystems and systems. These efforts are carried out through the technical direction of DOE and its network of national laboratories who work with private industry. Together they have established a comprehensive, goal directed program to improve performance and provide technically proven options for eventual incorporation into the nation's energy supply.

To be successful in contributing to an adequate national energy supply at reasonable cost, solar thermal energy must eventually be economically competitive with a variety of other energy sources. Components and system-level performance targets have been developed as quantitative program goals. The performance targets are used in planning research and development activities, measuring progress, assessing alternative technology options, and making optimal component developments. These targets will be pursued vigorously to insure a successful program.

CHAPTER 1

INTRODUCTION

The heat transfer surface of solar central receivers is generally made up of a bank of vertical tubes. Various heat transfer fluids (such as molten salt, water/steam, and air) flow through these vertical tubes, removing heat from the asymmetrically heated tube walls. When buoyant forces are in the direction of forced flow (upflow heating), the fluid velocity near the heated tube surface is augmented resulting in higher heat transfer rates. When buoyant forces are in the opposite direction of forced flow (downflow heating), fluid velocity near the heated tube surface slows or stagnates reducing significantly the rate of heat transfer. This investigation originates from considerations of this heat transfer effect and flow mechanisms in solar central receiver applications.

The stability of flow in a circular tube is influenced by hydrodynamic and/or thermal effects (1). Thermal effects, due to the heat transfer between the fluid and a bounding surface, often depend on both free and forced convection. Free convection heat transfer occurs when fluid motion is caused by buoyant forces. Forced convection occurs when fluid motion is produced by a pump, static pressure head or similar means.

When buoyancy effects are significant, secondary flows created by both free and forced convection distort the isothermal velocity profile causing instabilities in the flow. These instabilities can cause a laminar flow to undergo a transition process of thermal character (2).

For uniform heating of a fluid flowing upward in a vertical tube, particles near the wall are heated and the local fluid density decreases (see Figure 1). This results in a buoyant force, which increases the velocity of the flow near the heated tube wall. To satisfy continuity, flow in the center of the tube slows and in extreme cases may even reverse in direction.

For downflow with uniform wall heating, buoyant forces are in direct opposition to the direction of forced flow (see Figure 2). Fluid

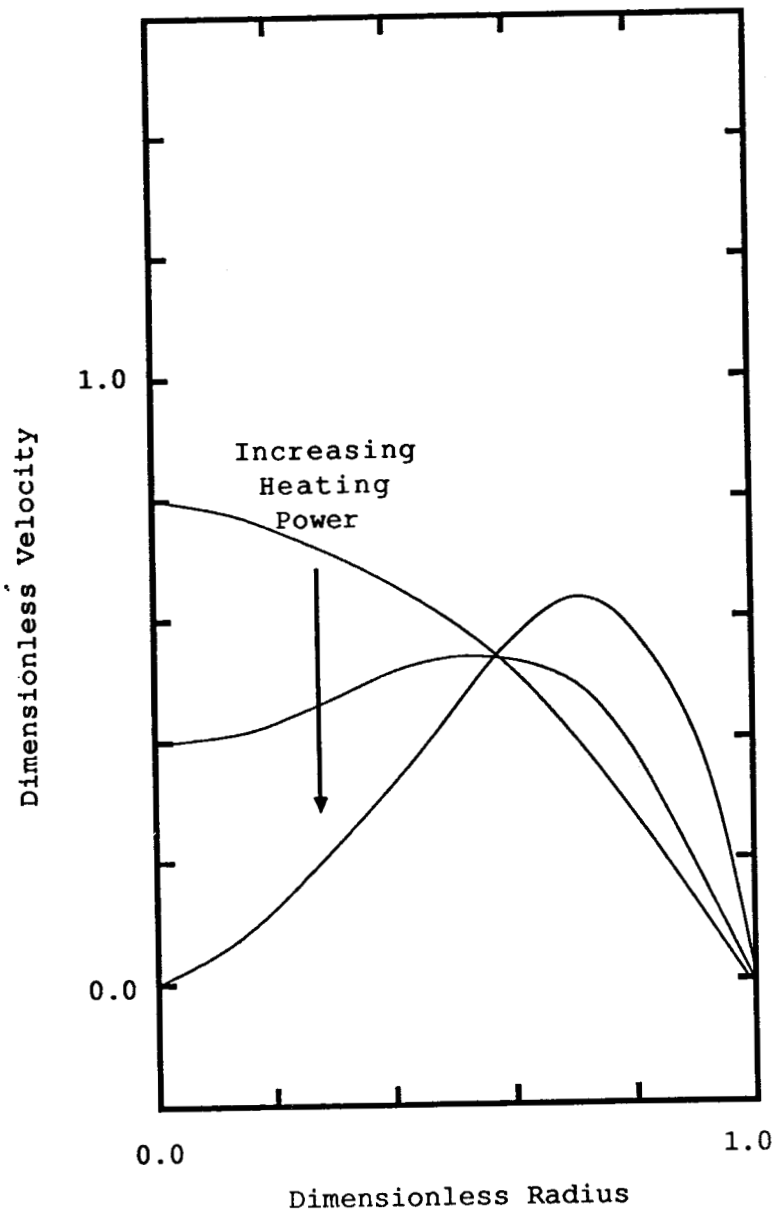

Figure 1. Upflow Velocity Profile

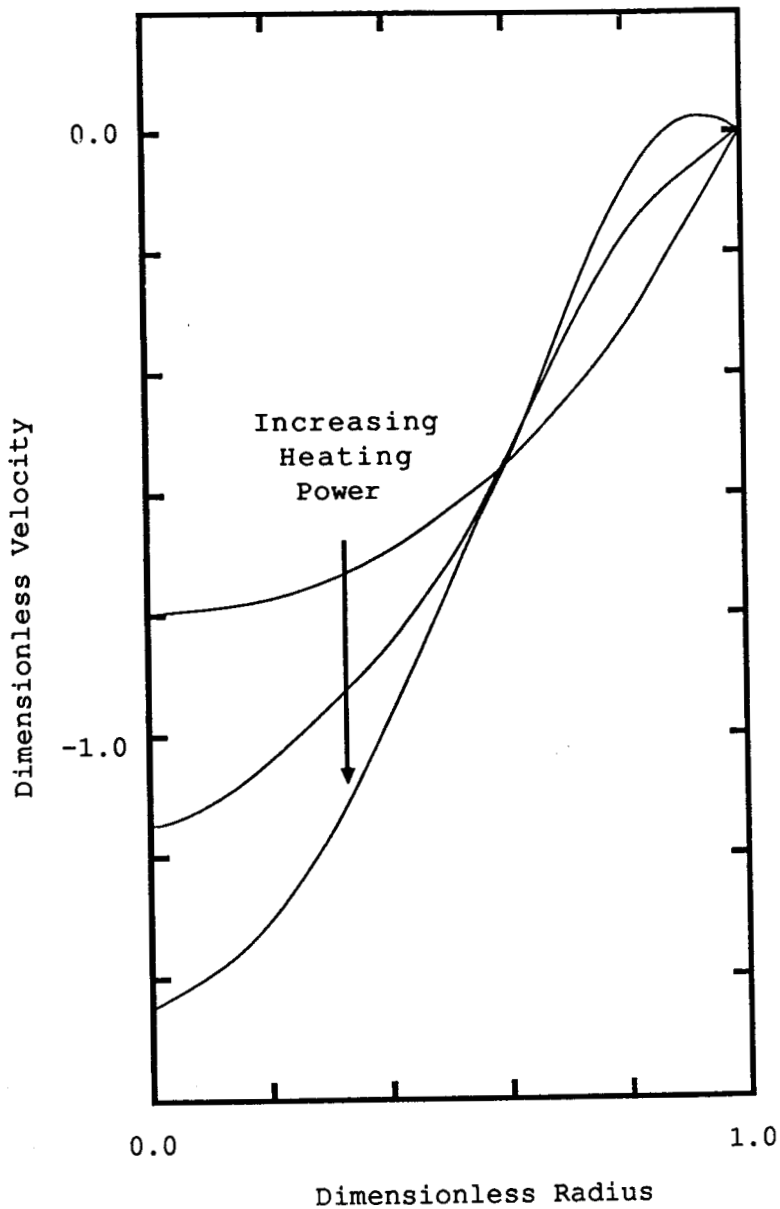

Figure 2. Downflow Velocity Profile

particles near the wall decrease in velocity and may reverse in direction, while flow in the center of the tube speeds up. Generally speaking, heat transfer rates are higher in upflow than in downflow heating (3).

For the flow condition in which both free and forced convection effects are significant, the Rayleigh and Reynolds numbers are used to characterize the flow regime. The Rayleigh number is defined as the ratio of the buoyant to viscous forces.

This present investigation is concerned with the effects of both free and forced convection on internal flow stability and the rate of heat transfer. The geometry and flow conditions studied experimentally are downflow heating in a vertical tube with a uniform wall heat flux applied to one-half of the tube perimeter. Laminar, transition and turbulent flow regimes were studied. Water is used as the heat transfer fluid.

Representation of experimental data is expressed in terms of these dimensionless groups (1):

$Nu = Nu(Re,Pr)$ forced flow

$Nu = Nu(Ra,Pr)$ natural flow

$Nu = Nu(Re,Ra,Pr)$ mixed convection,

in which

Nu = Nusselt number = hD/k

Re = Reynolds number = $(\rho VD)/\mu$

Pr = Prandtl number = ν/α

Ra = Raleigh number = $[g\beta(\Delta T/\Delta x)D^4]/(\nu\alpha)$.

In the above: k, ρ, μ, ν, α, and β are the fluid thermal conductivity, density, absolute viscosity, kinematic viscosity, thermal diffusivity, and volume expansion.

Related work reported in the literature is reviewed, followed by a description of the experimental apparatus. The experimental procedure used in this investigation, as well as the stability and heat transfer

results, are presented. Finally, conclusions and recommendations are discussed.

CHAPTER 2

LITERATURE REVIEW

Mixed convection heat transfer in a vertical tube or channel has received much attention in the literature (4, 5, 6, 3).

Considerable analytical and experimental work has been done for flow in a tube with a uniform wall heat flux. However, little attention has apparently been given to nonuniform wall heat flux cases (7, 8). This boundary condition is of particular interest in a variety of solar thermal applications where free convection (due to circumferentially nonuniform tube wall heating) has a considerable effect on flow stability and the rate of heat transfer.

El-Hawary (2) and Nagendra (9) studied the interaction of free and forced convection in horizontal tubes and its effect on flow stability and heat transfer. Both investigations utilized fluctuations in fluid temperatures and pressure drop to study the transition regime.

Stability maps were developed using transition data. Nagendra identified two types of transition flows and defined them in terms of intermittency factors (the period of time fluctuations are present to the measurement time period and the ratio of the fluctuation amplitude to the maximum fluctuation amplitude at transition).

El-Hawary defined "disturbed flows" as fluctuating flows exhibiting laminar-like friction factors. El-Hawary's description of "disturbed" flow and his presentation of transition data in terms of a stability map are used in the present study.

Kalinin and Yarko (10) investigated flow pulsations in heat transfer experiments and their effects on wall temperature. Fluctuations in wall temperature were periodic in nature with frequencies in the range 0.1 - 5.0 Hz.

Scheele (5) also used fluid temperature fluctuations to study the transition regime. The frequency of these fluctuations was also in the range 0.1 - 5.0 Hz.

The present investigation uses a thermocouple fluid probe and a differential pressure transducer to measure fluctuations in fluid

temperature and pressure drop across the test section. The thermocouple probe, pressure transducer, and the data acquisition system were capable of measuring fluctuations in the frequency range 0.1 - 10.0 Hz (see Sections 3.5 - 3.8).

McCoy (3) studied the downflow heating of water through a vertical tube at low Reynolds numbers and constant wall temperature. McCoy found Nusselt numbers for downflow were below those for pure free convection and much below those for upflow investigations reported in the literature. The Reynolds number varied from 200 to 6,000. The heat transfer section in McCoy's experiments had a length-to-diameter ratio of 120. Heat transfer coefficients were determined and the Nusselt number was graphically correlated as a function of Grashof, Prandtl and Reynolds numbers. Hallman (4) presented analytical and experimental results of laminar flow for both upflow and downflow. The heat transfer section had a length-to-diameter ratio of 115. The Reynolds number varied from 27 to 3,300, and the Rayleigh number ranged from 27 to 2,700. Heat transfer data were graphically presented in terms of Nusselt number versus Rayleigh number. In upflow, Hallman observed a transition from steady laminar flow to a slow, random, eddying flow with increasing power. For downflow runs, asymmetries in wall temperatures became more severe as the heating power was increased. For the highest heating levels the flow became unsteady and wall temperatures oscillated periodically at a frequency of about 1.3 - 1.7 Hz. Variations of as much as 20 °C were noted in wall thermocouples located at the same axial location, but at opposite circumferential locations. A stability correlation, above which transition to an unstable flow occurs, was given in (4)

$$Ra = \{[\rho^2\beta g(Tw-Tm)D^3]/\mu^2\}Pr = 9470[(RePr)/(2x/D)]. \qquad (1)$$

Hanratty, Rosen and Kabel (6) used visual dye experiments to illustrate the distorted velocity profiles resulting from the heating or cooling of water flowing in a vertical tube. The test section had a length-to-diameter ratio of approximately 100. Experiments were performed at low Reynolds numbers (Re = 125). Their experiments indicated that instabilites in the flow were caused by changes in the

density gradient near the wall, and not by variations in viscosity (since their results depended on whether natural convection aided or opposed forced flow). For sufficiently large heating rates in upflow the isothermal, parabolic velocity profile was distorted so that the velocity near the wall increased.

This resulted in the slowing and eventual reversal of flow in the center of the tube. This inverted flow region became turbulent downstream. For sufficiently large cooling rates in upflow (or heating in downflow) fluid near the wall slowed down, resulting in an increase in velocity near the center of the tube. Flows became unstable when a reversal of flow occurred at the wall. Hanratty, Rosen and Kabel (6) also presented an analytical solution for constant wall heat flux. These solutions were limited to fully developed velocity and temperature profiles far downstream from the beginning of the heat transfer section. For heating in upflow, flow reversal occurred at the center of the pipe for $Gr/Re > 122$. For cooling in upflow, for $Gr/Re = 42$ the velocity gradient at the wall vanished and an unstable flow condition existed as cited in Schlicting (11). The analysis of Hanratty, Rosen and Kabel (6) demonstrated that the observed distortions in the flow field could be explained by natural convection effects.

Scheele, Rosen and Hanratty (12) studied the transition regime at low Reynolds number for water flowing in a vertical circular pipe. Both upflow heating (natural convection in the direction of forced flow) and upflow cooling (natural convection opposed to forced flow) were studied. Constant wall temperature and constant heat flux boundary conditions were also investigated. The heat transfer section had a length-to-diameter ratio of 114. The experiments were performed under conditions that satisfied the Boussinesq approximation (constant-property assumption except for the density difference, which generates the buoyancy force). Results for constant wall heat flux in upflow showed that the first indication of instability was a sinuous motion of the dye filament. This sinuous motion gradually grew with decreasing Reynolds number until the dye filament broke up completely (as forced convection effects decreased and the influence of free convection effects increased). For constant flux heating in downflow, instability was

first observed as a slight asymmetry of the dye filament followed by intermittent bursts of highly disturbed flow. As the Reynolds number decreased, the frequency of these bursts of disturbed flow increased. Transition for upflow heating occurred gradually, whereas transition for downflow heating appeared to occur much more suddenly. For upflow heating, instabilities occurred when the maximum local fluid velocity no longer occurred at the center of the pipe. For downflow heating, transition did not occur until there was flow reversal at the pipe wall.

Scheele and Hanratty (13) considered the range of Reynolds numbers (up to 1,800 for upflow and up to 4,700 for downflow) in longer heat transfer sections (length-to-diameter ratios of 305, 610,and 762). Experiments were carried out using a constant wall heat flux boundary condition. Fluctuations in fluid temperatures, measured by a thermocouple inserted near the downstream end of the tube, aided in detecting transition. Both upflow and downflow heating were considered. For upflow heating, flow first became unstable when the velocity profile developed a point of inflection. Gradually, small disturbances grew culminating in disturbed flow. For downflow heating, instabilities were associated with flow separation at the tube wall. Unsteady flow developed suddenly after this unstable condition occurred. Scheele and Hanratty suggested that the intermittent character of the temperature fluctuations could be caused by a mechanism similar to the alternating separation and reattachment process discussed by Guerrieri and Hanna (14).

Guerrieri and Hanna (14) investigated air flowing downward in a vertical channel with a symmetric constant wall heat flux. In some tests, a transition to turbulent flow occurred that was marked by an increase in the heat transfer rate in the channel. Data indicated a critical Gr/Re of approximately 25. This ratio is in agreement with Hanratty, Rosen and Kabel whose analytical results found a critical Gr/Re of 21. At low flow velocities natural convection effects dominated forced convection effects. Buoyant forces caused air near the heated channel walls to flow upward, while the airstream as a whole flowed downward. At high flow velocities all flow was downward. At the highest mean velocity the local heat transfer coefficient agreed with

laminar flow theory (neglecting natural convection effects). Guerreri and Hanna suggested that when flow reversal occurs, a 'turbulent-like' condition exists so that the heated layers push into the core of the gas stream. This brought the core temperature much closer to the wall fluid temperatures. Since the buoyant effect depended on the density difference, a decrease in the velocity of the gas near the wall resulted. This slowing of the flow again reduced heat transfer. It was also found that local heat transfer coefficients fluctuated with time. Very little analytical or experimental work is available on flow through a pipe or channel with asymmetric wall heating.

Siegel, Sparrow and Hallman (15) presented an analytical solution for flow in a horizontal tube with prescribed wall heat flux. They generalized the solution for uniform wall heat flux to solve for the case of nonuniform wall heat flux.

Reynolds (16) performed an analysis, assuming constant fluid properties, for fully developed laminar flow in a vertical circular tube with a circumferentially nonuniform wall heat flux. His results indicated circumferential variations in wall heat flux can significantly affect the rate of heat transfer. Reynolds (17) also considered turbulent flow for the same conditions. The latter analysis predicted temperature variations around the tube for nonuniform wall heat fluxes. Reynolds' analysis showed that the effect on heat transfer in turbulent flows, for nonuniform wall heating, was more pronounced than in laminar flows.

Sparrow and Black (8) experimentally and analytically studied the heat transfer effect of asymmetric heating on turbulent flow (circumferentially varying wall temperature and wall heat flux). Air was used as the heat transfer fluid. Generally, higher local Nusselt numbers were found near circumferential locations of lesser heating, whereas lower Nusselt numbers were found near locations of higher heating.

Schmidt (7) investigated effects of asymmetric heating in a horizontal tube flow. The experimental study was concerned with heating the top of the tube wall and included results over a large range of turbulent flow Reynolds numbers. Schmidt found large circumferential variation of local heat transfer, with an apparent negligible effect of

buoyant forces.

This investigator was not able to find any experimental work concerning flow through a vertical tube with a similarly applied asymmetric wall heating condition.

CHAPTER 3

EXPERIMENTAL PROGRAM

3.1 TEST CONFIGURATION

A diagram of the experimental apparatus is shown in Figure 3. The heat transfer medium used was tap water, which was first passed through a 0.10-micron filter. A Temptrol water chiller, having an insulated 55-gallon tank, was used to hold and pump incoming water up to an overhead tank. Originally, the water chiller was to be used to chill the water down to the designated inlet temperature. Because of recurring maintenance problems this unit was used only as a pump and holding tank. The inlet water temperature varied ±0.2 °C over a test period of approximately 2 hours.

Water was pumped from the Temptrol unit to a stainless steel tank located approximately 1.5 m above the apparatus. Constant flow conditions were maintained by the use of the head tank and an overflow drain. The drain was located near the top of the tank and kept the water level constant.

Inlet water temperatures were measured by a thermocouple submerged near the exit of the head tank. Isothermal flow tests revealed differences between head tank temperatures and wall temperatures (located near the inlet to the test section) of less than ±0.1 °C. Therefore, the reported inlet temperature was actually the measured head tank temperature. The entrance of the exit tube for the head tank was located a distance of about 0.1 m from the bottom of the head tank. This was to prevent any sediment, which may have settled to the bottom of the head tank, from entering the test section and affecting flow.

Water from the head tank flowed down a 1.22-m section of 9.5-mm (inside diameter) flexible tubing before passing into the smooth inlet of the hydrodynamic approach. Water flowed from the hydrodynamic approach into the test section, then into the exit section and through a needle valve. The needle valve was used to vary the flowrate. Flowrates were determined by collecting a known quantity of water over a measured time period. After water passed through the needle valve, it was

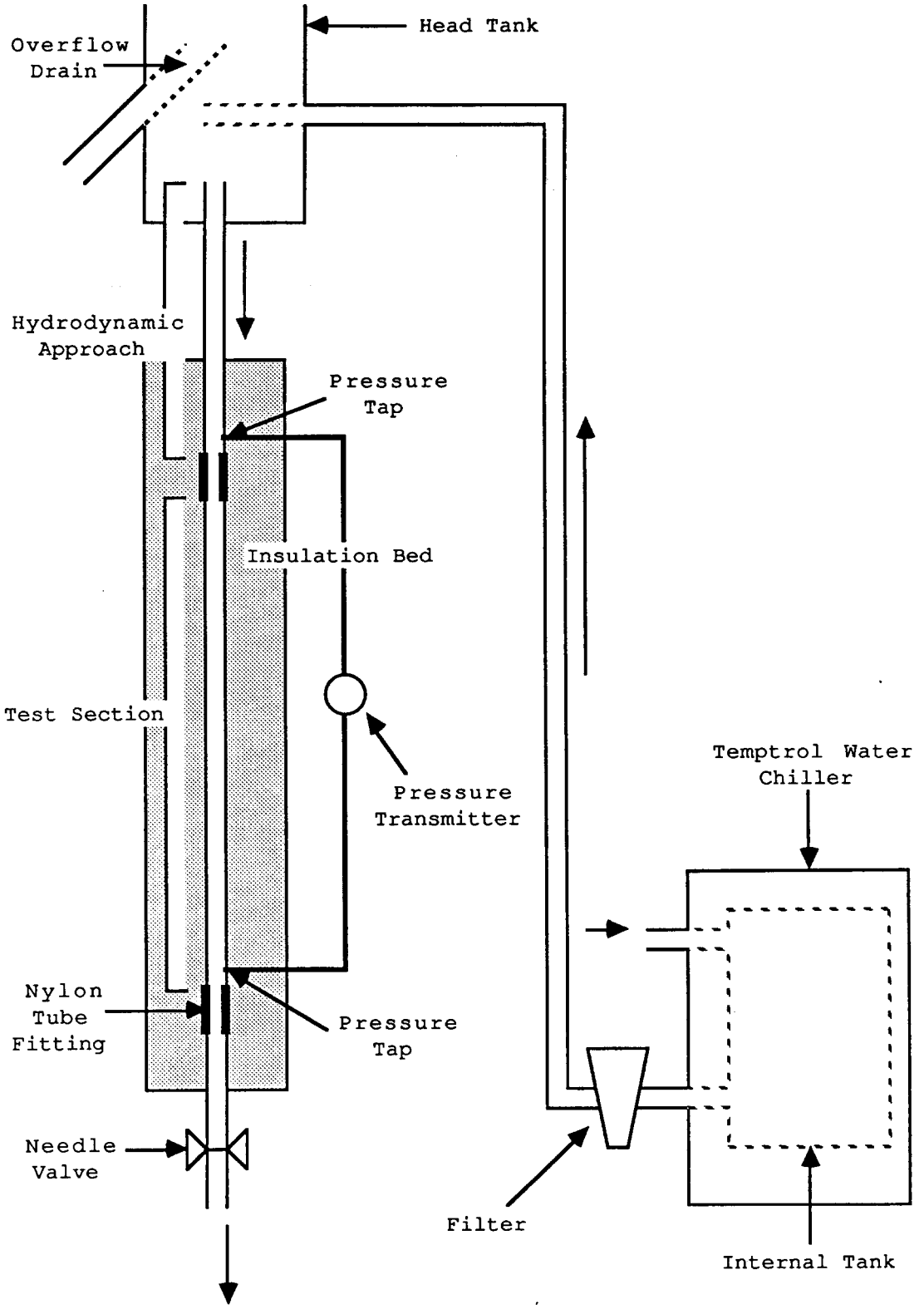

Figure 3. Diagram of Test Configuration

discarded (see Appendix B for error analysis).

The hydrodynamic approach, test section, and exit section were heavily insulated to isolate the experiment from fluctuating ambient temperatures. The hydrodynamic approach had a length-to-diameter ratio of 150. This length allowed the velocity profile to become fully developed.

The test section was separated from the hydrodynamic approach, pressure tap, and exit section by nylon tube fittings. These fittings provided approximately 24 mm of nylon between metal tube ends. This effectively isolated the heated test section and reduced the conduction losses to unheated sections of the apparatus. The tube fittings were also counterbored to assure a smooth flow passage between tube sections.

3.2 TEST SECTION

The hydrodynamic approach, test section and exit section were made from a continuous length of stainless steel 304 tubing. The outside diameter was approximately 9.5 mm (0.375 inches) with a wall thickness of about 0.9 mm (0.035 inches). The length of the test section was approximately 2.18 m, which resulted in a length-to-diameter ratio of about 280. The outside diameter was examined for uniformity and accuracy over the whole length of the tube. The inside diameter and wall thickness were also examined at each end.

To simulate the asymmetric heat flux boundary condition, several flexible foil heaters were fitted in series to one-half of the test section tube wall (see Figure 4). The heaters were ordered with aluminum backings to more evenly distribute heat to the test section wall. This also resulted in a stiffer foil. These flexible heaters were attached using a self-adhering silicone rubber stretch tape. The stretch tape held the heaters in place and provided strong, even pressure neccessary for good thermal contact between the aluminum backing of the heaters and the outer tube wall.

Pressure taps, located at the end of the hydrodynamic approach and at the end of the test section, were silver-soldered to the tube wall.

A 36-gage thermocouple probe was placed one-quarter radius into the flow, on the heated side of the tube, after the last heater. This probe was used to measure fluctuations in fluid temperatures.

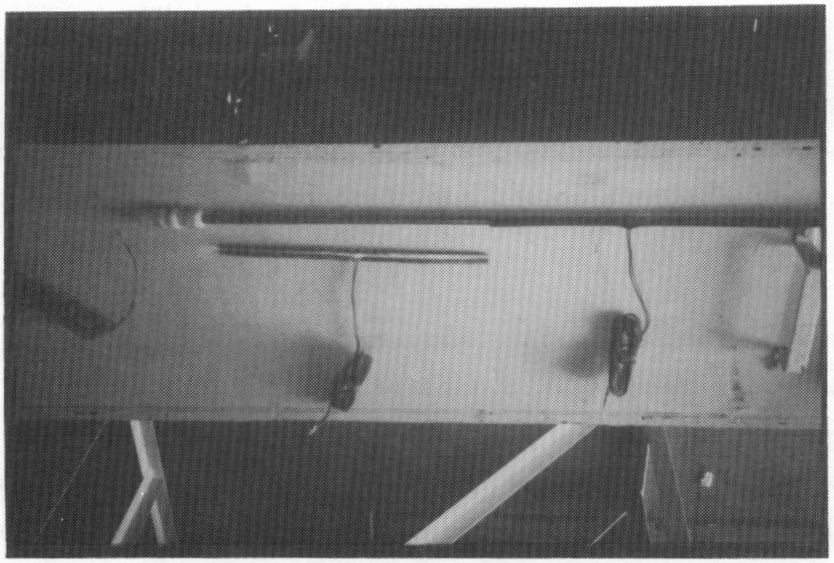

Figure 4. Details of Test Section

Local wall temperature measurements were made by thermocouples embedded in the tube wall. Using a drill press, a small hole was drilled approximately half-way into the tube wall. This was done at every wall thermocouple location. Each thermocouple bead was then centered in the hole and epoxied in place. Slight downward pressure was applied to the thermocouple wire throughout the curing process. This insured that the bead remained centered in the hole and was in good contact with the wall of the tube.

Thermocouples were axially spaced 273 mm apart at the middle of the test section and as close as 13 mm apart at the ends of the test section (see Appendix A for actual locations). Thermocouples were generally placed on the side of the tube wall, at the edge of the heaters, and alternated sides along the length of the test section.

At three locations (one near each end and one in the center of the test section), four thermocouples were placed around the entire tube perimeter to evaluate the effect of heater positioning (see Figure 5 for details of thermocouple tube positions). All thermocouples were referenced to a common terminal block. The terminal block was referenced to 65 °C electronically.

3.3 TEST SECTION INSULATION BED

The hydrodynamic approach and the test section were insulated from ambient conditions by 0.15 m of ceramic insulation board having a thermal conductivity of 0.5 W/m °C. A 0.15-m by 0.30-m by 3.0-m plywood channel was filled with ceramic board to form the insulation bed. The hydrodynamic approach, test section and exit section were all fitted in place down the center of the bed (see Figure 6). A similar piece (0.16 m by 0.30 m by 3.0 m), divided into three sections, was then fitted on top of the bed. This sandwiched and isolated the entire flow apparatus from ambient conditions. Turnbuckles were used to compress the two halves together. Tape was used to seal any air gaps between bed surfaces and to restrict air movement between bed pieces (see Figure 7).

The test-bed support structure was made up of welded angle iron and was designed to allow the test bed to rotate between the horizontal and vertical positions. In the horizontal position the test bed could be opened up and worked on easily. Then it could be closed up and rotated

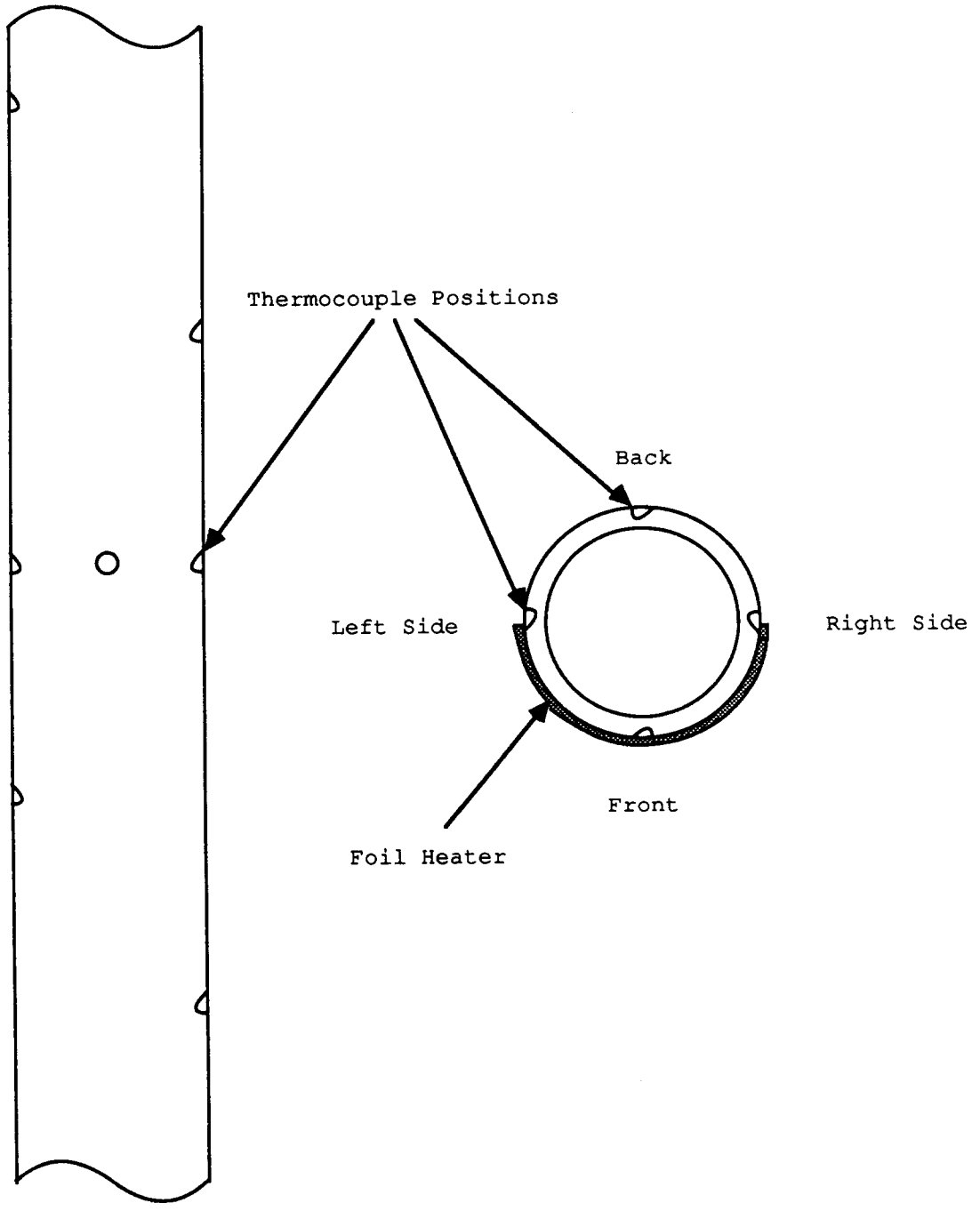

Figure 5. Thermocouple Locations On Tube Perimeter

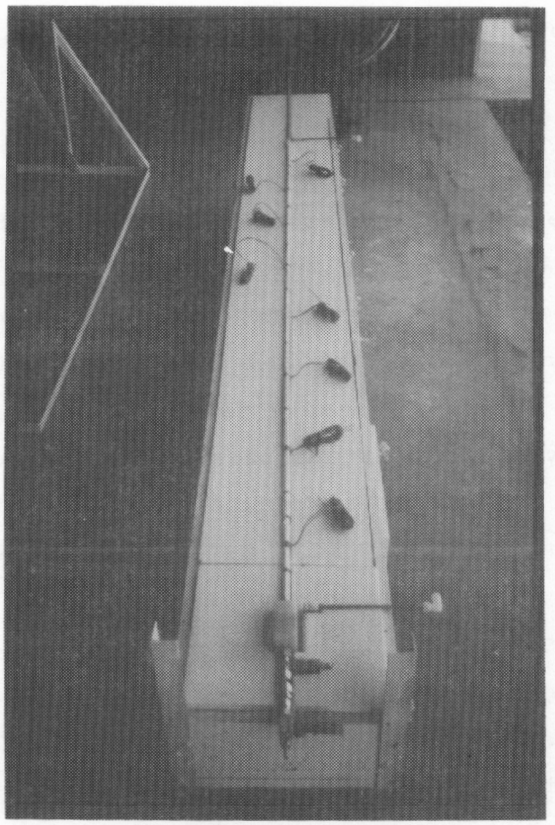

Figure 6. Test Apparatus

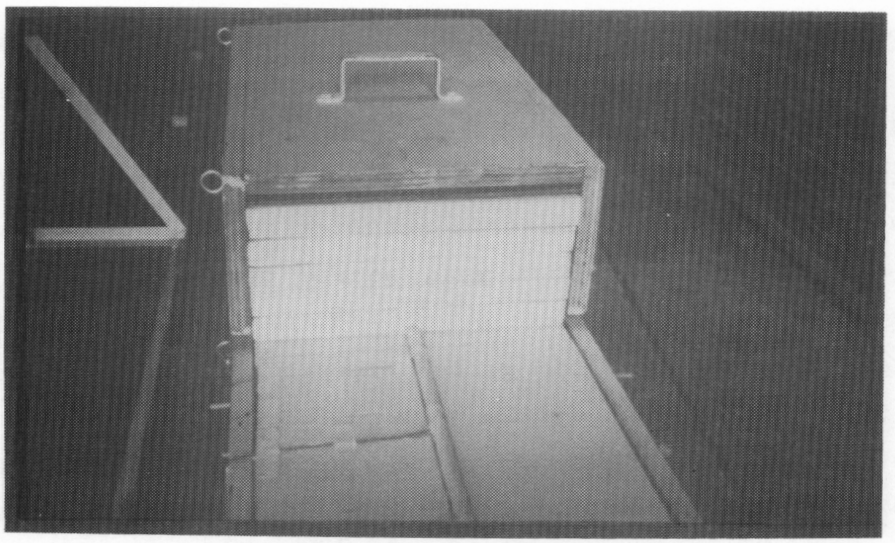

Figure 7. Test Section Insulation Bed

to the vertical position for testing purposes.

3.4 EXPERIMENTAL PROCEDURE

Tests were performed using the following experimental procedure. After allowing the water temperature to stabilize (approximately 1 hour) the holding tank was slowly filled. The holding tank was then left to stand for 15 minutes in order to remove any entrapped air. The head tank was then filled from the bottom and left to sit with a slight overflow for about 1 hour. Next the needle valve, controlling flow to the test section, was fully opened for approximately 15 minutes. All the above steps were followed in order to reduce the level of air in the holding tank and apparatus. After these steps, the head tank was visually inspected for air. This process removed most of the air from the system. The apparatus was now ready for testing.

Initial flowrates and power levels were set and the apparatus was allowed to reach approximate steady-state conditions. This approximate steady-state condition was determined when the outlet bulk fluid temperature varied by no more than 1 °C over a period of 1 hour. Next the flowrate was determined by measuring the time it took to fill a 1 liter graduated cylinder (approximately 1.5 minutes). Flowrate measurements were repeated at least three times to obtain averages for the mass flow.

After the velocity was determined, the data acquisition sequence was begun. First the wall and inlet thermocouple voltages were measured, followed by the fluid probe and pressure transducer signals. The fluid temperature and pressure data were taken sequentially. A statistical analysis was performed after each measurement period. This analysis consisted of calculating root mean square percent fluctuations (rms fluctuation, $\sqrt{P'^2} / \bar{P}$ and $\sqrt{T'^2} / \bar{T}$). Rms fluctuations were calculated for both the fluid probe temperature and the pressure drop. Sample sizes were 340 readings for each calculation.

The thermocouple fluid probe and the pressure transducer signals were next recorded, side-by-side, on a Honeywell Visicorder. This device had a frequency response of 0.1 - 50 Hz. These measurements were recorded for approximately 3 minutes. This provided a side-by-side, visual description of the fluid temperature and pressure drop

fluctuations.

For each data point three complete sets of data were taken to check for reproducibility. These three sets of data were later averaged and reduced to one set of data.

After all data were recorded for a given test point, the flowrate or power level was set to the next test level. A minimum stabilization period of 1 hour was allowed between test points.

In tests 1 through 5, heating power was held constant while flowrate was allowed to incrementally increase until the flow became turbulent. This was accomplished through a succession of approximate steady-state steps, each lasting no less than 1 hour. In tests 6 through 9, the flowrates were held constant while the heating power was similarly increased stepwise.

3.5 DATA ACQUISITION SYSTEM

Thermocouple and pressure transducer emf outputs were monitored by a Hewlett-Packard 3456A DMM, which was controlled by a Hewlett-Packard 9845 computer. Specifications for the HP 3456 DMM indicate resolution to 0.1 v (18). This corresponds to an accuracy in temperature measurement of better than ±0.02 °C (for copper-constantan thermocouples).

3.6 TEMPERATURE MEASUREMENT SYSTEM

Thirty-six-gage copper-constantan thermocouples were used for all temperature measurements except for the outlet bulk fluid probe (a 12-gage thermocouple probe). A Hy-Cal reference junction with a reference temperature of 65 °C ±0.02 °C (19) was used at the copper-to-constantan, copper-to-copper interface. The 36-gage thermocouple used for the fluid probe had a frequency response of approximately 0.1 - 10.0 Hz (20).

3.7 PRESSURE MEASUREMENT SYSTEM

Pressure drop across the length of the test section was measured by a Rosemount Model 1151 DP Alphaline Differential Pressure Transducer. The frequency response of the pressure transducer was approximately 0.1 - 5 Hz (21).

3.8 DESCRIPTION OF HEATER CIRCUITS (HEAT FLUX SOURCE)

Eight 273-mm by 15-mm, flexible foil heaters manufactured by Minco Products Inc. were used to simulate the nonuniform wall heat flux. All heaters had aluminum backings to uniformly distribute the heat flux over the outer tube surface. The heaters were manufactured with 20-gage lead wires (7 amp maximum current) and were rated up to 50 W/m^2. Their resistances were determined to be within 1 percent of each other. To accommodate the anticipated power consumption requirements, two series circuits (four heaters each) were powered by two Sorensen DC power supplies. Voltages were measured by the HP 3456A DMM.

CHAPTER 4

RESULTS AND DISCUSSION

Stability and heat transfer data were obtained for water flowing downward in a vertical tube with a constant wall heat flux applied to one-half of the tube perimeter. The range of the Reynolds numbers considered was $1,200 < Re < 4,000$. The range of the Rayleigh numbers was $40 < Ra < 1,030$. Because the hydrodynamic approach had a length-to-diameter ratio of about 150, the flow was considered fully developed upon entering the test section.

Flow friction factor, heat transfer coefficient, and pressure and temperature fluctuations were examined to determine the flow regime of each data point. This is illustrated in Table 1. The statistical rms fluctuations and side-by-side fluctuation output from both the fluid temperature probe and the pressure transducer (see Appendix A) aided in defining each data point.

Friction factors were calculated (using the Darcy-Weisbach formula) by measuring the pressure drop across the test section. Heat transfer coefficients were calculated using average wall and bulk fluid temperature differences and the power put into the fluid. As mentioned in Section 3.4, continuous fluid temperature probe and pressure transducer signals were transmitted to a Honeywell Visicorder and recorded, side-by-side, for a period of about 3 minutes. These fluctuation time histories (see Appendix A) allowed fluctuations in fluid temperature and pressure drop to be visually studied and compared. Rms fluctuations were calculated by taking approximately 340 readings at sample rates of twenty readings per second and forty readings per second (a 17-second and an 85-second measurement period). Two sampling rates were utilized to determine periodicity of the fluctuations. Neither sampling rate accounted for the high frequency fluctuation spectrum. However, the two sampling rates did show that the measured fluctuations are of relatively low frequency, in the range of 0.1 - 5 Hz.

The laminar flow region was characterized by laminar friction factors, following Hagen-Poiseuille flow theory ($f = 64/Re$), Nusselt

Flow Regime	Temperature Fluctuation (peak to peak) Amplitude	Period	Pressure Fluctuation (peak to peak) Amplitude	Period	Friction Factor, f	Nusselt Number
Laminar	none		none		followed Hagen-Poiseuille Flow Theory	5.5 > Nu
Disturbed	20 - 31 °C	20 - 52 s	40 - 150 Pa	20 - 52 s	followed Hagen-Poiseuille Flow Theory	7.0 > Nu > 5.5
Thermal Transition	5 - 21 °C	random*	18 - 179 Pa	random*	deviated from Hagen-Poiseuille Flow Theory	8.5 > Nu > 5.5
Hydraulic Transition	1 - 29 °C	random*	131 - 477 Pa	random*	deviated from Hagen-Poiseuille Flow Theory	8.5 > Nu > 5.5
Turbulent	1 - 3 °C	continuous, high frequency fluctuations	37 - 299 Pa	continuous, high frequency fluctuations	followed Blasius resistance formula	Nu > 8.5

*continuous, non-periodic fluctuations

Table 1. Summary of Flow Regime Characteristics

numbers below 5.5 and no fluctuations in fluid temperature or pressure drop. The disturbed flow region was characterized by laminar friction factors, Nusselt numbers in the range 5.5 to 7.0, measurable rms percent fluctuations and visually observed fluctuations in either the fluid temperature or the pressure drop.

Hydraulic and thermal transition regions were characterized by hydraulic-like transition friction factors and Nusselt numbers between 5.5 and 8.5. Large rms fluctuations and continuous fluctuations in both the fluid temperature and the pressure drop were also observed. It should be noted that the maximum fluid temperature fluctuation (as measured by both rms fluctuation and fluctuation time histories) occurred at the onset of transition and decreased to a steady higher frequency fluctuation level in turbulence. Maximum pressure drop fluctuations always occurred after the fluid temperature fluctuations had peaked (see Appendix A).

The development of fluctuations in both the fluid temperature and the pressure drop were precisely monitored by both the calculated rms data and the fluctuation time histories.

The turbulent region was characterized by turbulent friction factors, which gradually decreased with increasing Reynolds numbers.

Nusselt numbers for turbulent flow were above 8.5, and all fluctuations decreased dramatically in amplitude to a steady higher frequency level.

A stability map (Figure 8) was constructed to describe flow regions corresponding to a variety of thermal and hydrodynamic flow conditions. Flow regimes (laminar, disturbed, transition, and turbulent) were identified using the criteria discussed above.

Flows with velocities under 0.3 m/s progressed in character from a laminar flow to a disturbed flow with increasing heating power (see Figure 8). As heating power continued to increase, this disturbed flow became transition-like in character. This apparent thermal transition had all the characteristics of the usual hydraulic transition. Some local wall temperatures were, however, above boiling. Air was also noted in the effluent at these higher power levels. Therefore, it is not clear whether transition was caused by thermal instabilities or some other mechanism related to the conditions mentioned above. It should be noted

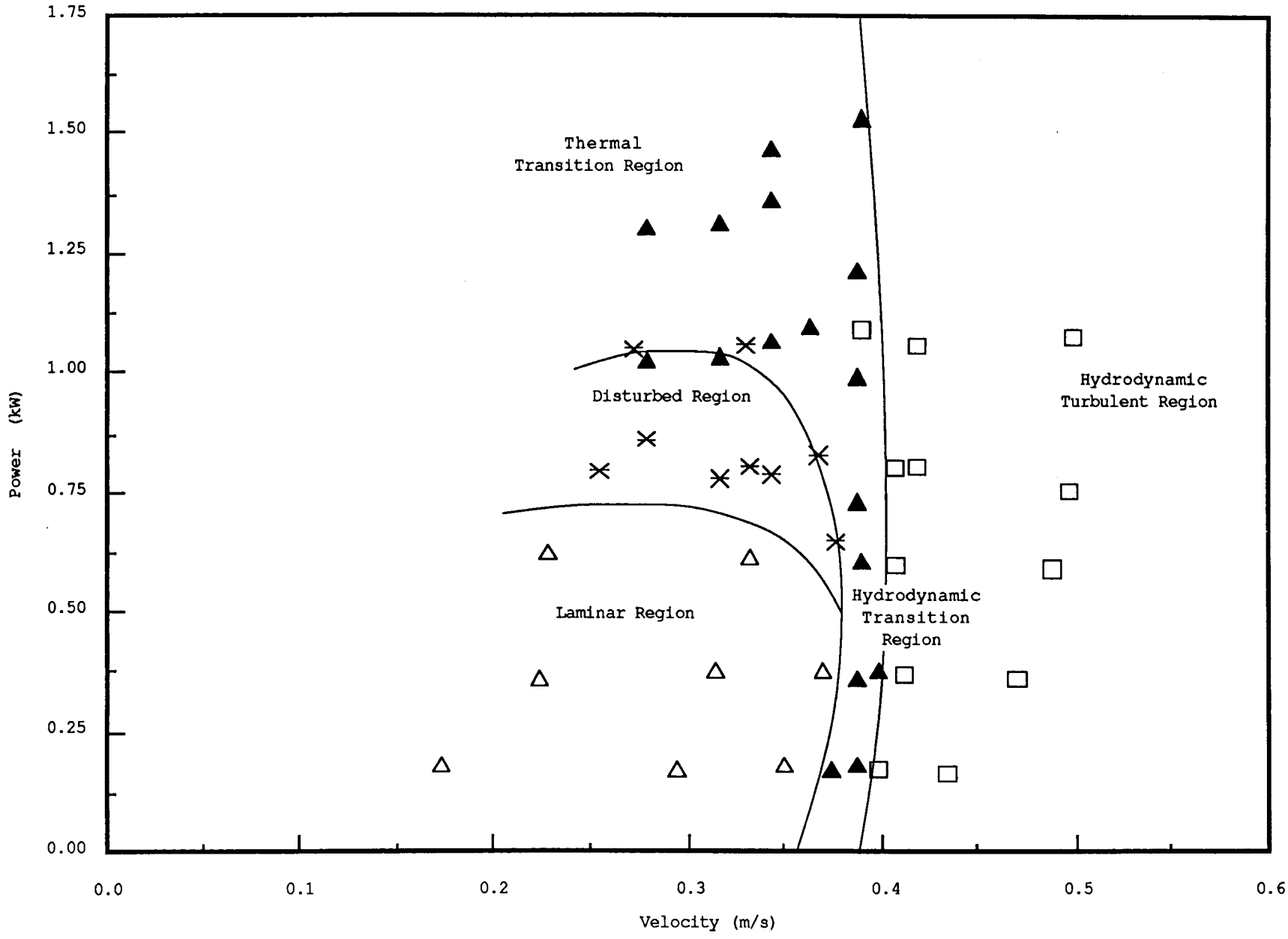

Figure 8. Flow Stability Map, Power vs. Fluid

that these experimental problems could be avoided in future works by using a heat transfer fluid other than water, such as an oil or glycol. These problems restricted the present investigation from studying the thermally turbulent region.

A representation of flow regime boundaries is shown in Figure 9. This figure, which is very similar and describes the same regions as Figure 8, shows that heating has a distinct stabilizing effect on flow at low Rayeigh numbers.

The isothermal and heated flow friction factors are shown in Figure 10. Figure 10 clearly shows the effect that heating has on stabilizing flows. As heating power increased from 0 to 1 kW, the critical Reynolds number increased from 2,400 to about 3,000.

Both El-Hawary (2) and Nagendra (9) noted this stabilizing effect at Rayleigh numbers below about 225 for flow through a horizontal tube with a uniform wall heat flux. However, at higher Rayleigh numbers the present investigation, as well as others, found instabilities caused by heating resulted in large fluctuations in fluid temperature and pressure drop. Increased heat transfer in El-Hawary (2) and in the present study was also noted. The character of the initial fluctuations was periodic and progressively grew in amplitude and frequency as a flow neared transition. During transition, both thermal and hydraulic, the amplitude of fluctuations decreased while the frequency continued to increase. As the flow became turbulent, fluctuations dampened even further to a low- amplitude, high-frequency level.

Figures 13(a) through (f) in Appendix A show the growth process of flow fluctuations as heating power was increased at constant flowrate. Similarly, Figures 14(a) through (f) show the growth process as flowrate was increased at constant heating power. Tests at constant flowrate progressed (with increasing power) to a thermal transition-like flow (2). As mentioned previously, this may not have been due only to thermal instabilities. The latter process progressed through a hydrodynamic transition region before becoming turbulent.

For all tests, fluctuations began periodically and increased in magnitude and frequency until transition (after which time, the magnitude of fluctuations decreased). It can been seen (see Appendix A) that bursts of disturbed flow passing down the tube are sensed by both devices

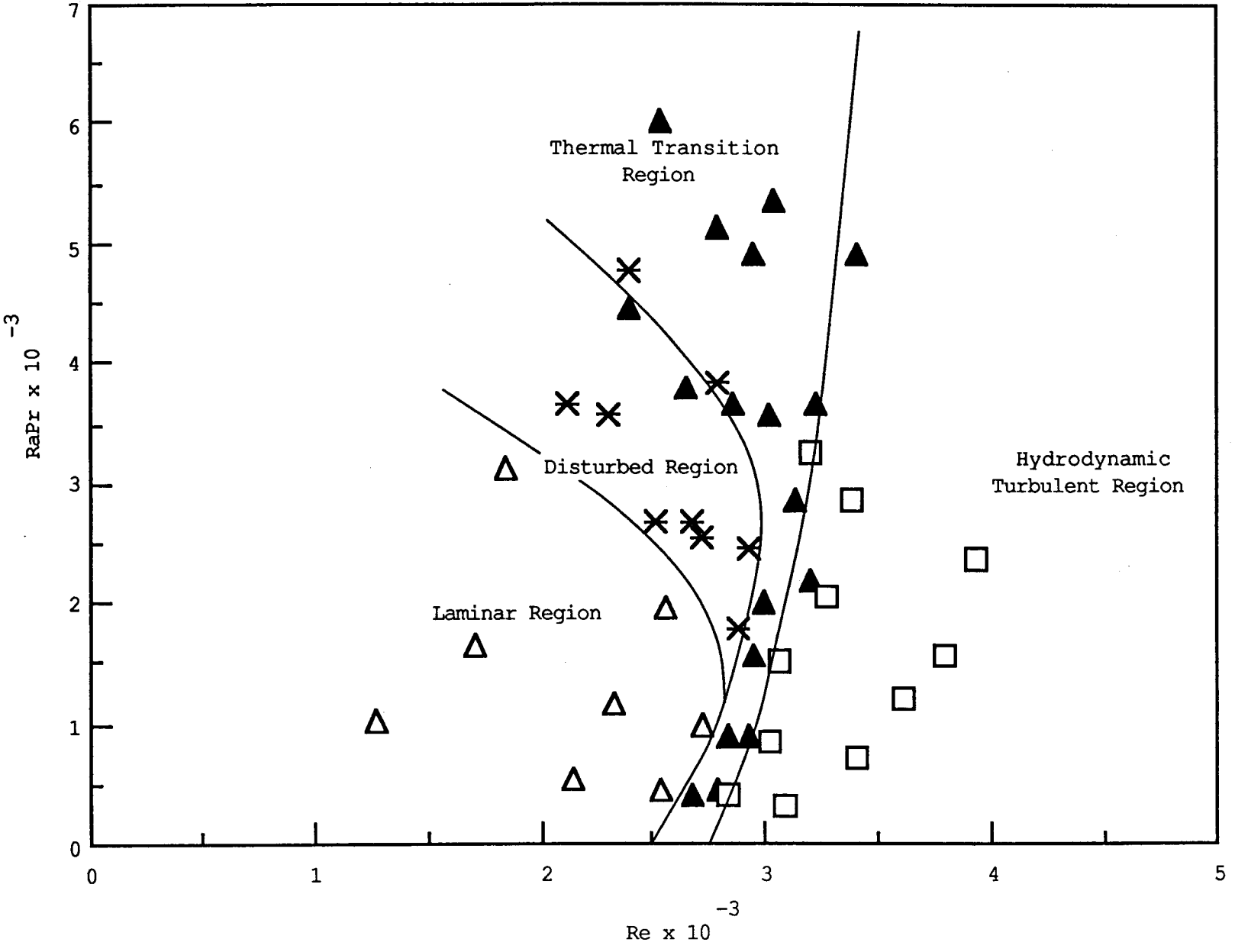

Figure 9. Flow Stability Map, RaPr vs. Re

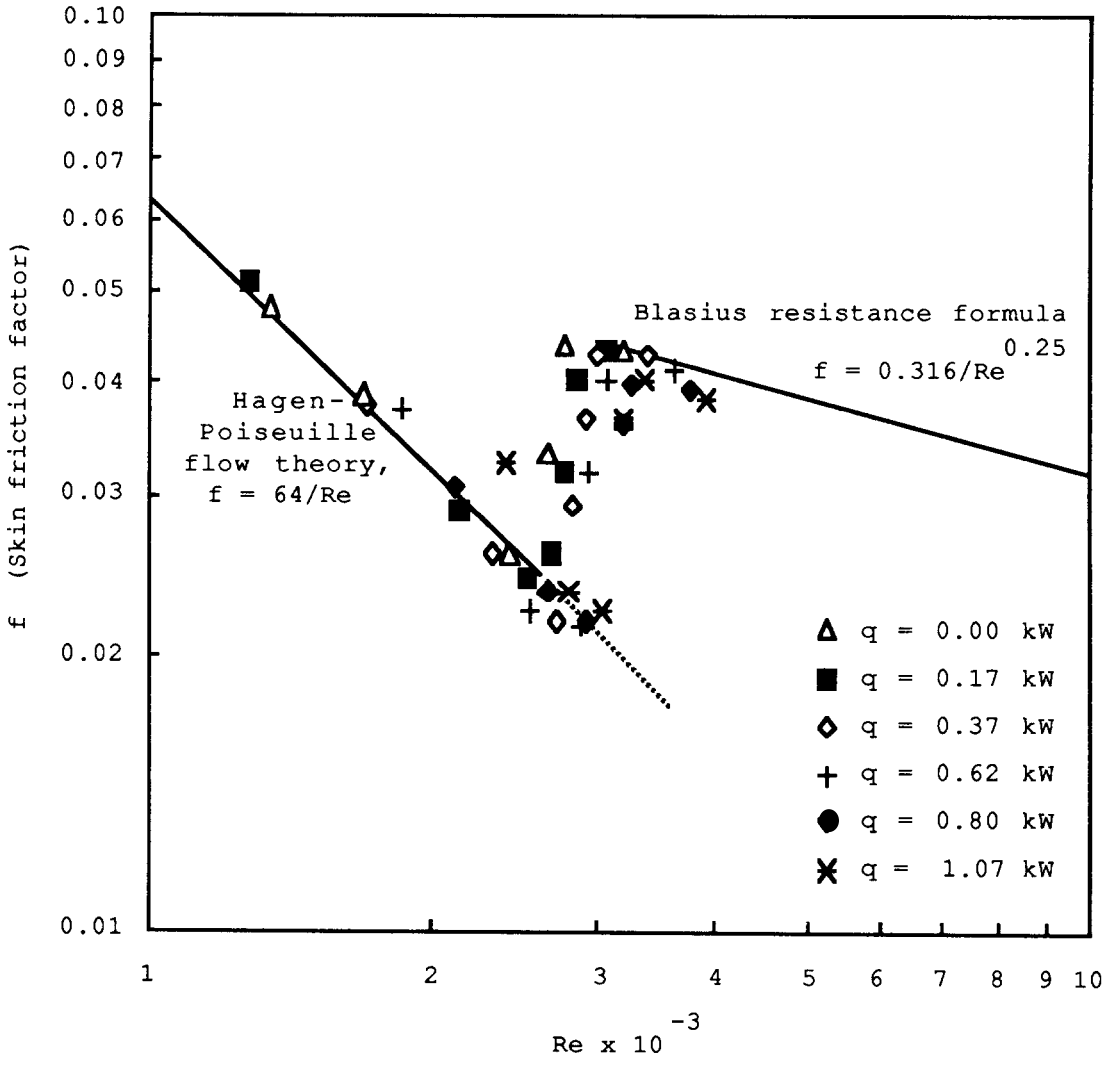

Figure 10. Plot of f vs. Re

at virtually the same time. The pressure transducer tended to sense a disturbance in flow just prior to the fluid temperature probe. This is what one would expect, because the fluid temperature probe was located at the outlet end of the test section.

Scheele and Hanratty (13) investigated the effect constant wall heat flux had on the stability of water flowing through a vertical tube. El-Hawary (2) made a similar study in horizontal tubes. Disturbed flows, that is flows in which fluctuations in fluid temperature were present, were considered unstable by the former authors and are the basis for the following comparison.

Instabilities in El-Hawary's horizontal tube flow, where buoyant forces were perpendicular to the direction of forced flow, were first noted at a Rayleigh number of about 200. Scheele and Hanratty's flow through a vertical tube became unstable at a Rayleigh number of approximately 1,500 for upflow and 2,000 for downflow. The present investigation noted unstable flow at Rayleigh numbers of around 500. Therefore, downward flow in a vertical tube with asymmetric wall heating is considerably more unstable than for the case of a uniform wall heat flux. However, this nonuniformly heated flow was still more stable than flow through a horizontal tube with a uniform wall heat flux.

Heat transfer data are presented first in terms of Rayleigh then Reynolds numbers. Figure 11 relates the Nusselt number and Rayleigh number at various Reynolds numbers. The lower curve denotes points at a Reynolds number of 2,000 and the upper curve at a Reynolds number of 3,500. The three curves between these limits represent all data points at a Reynolds number of 2,750. The lowest of these three curves reflects data for flows that have not undergone transition, as indicated by f, h, and rms fluctuation values. The middle curve represents flows in transition, and the last of these three curves represents flows at a Reynolds number of 2,750 that are turbulent in nature. Figure 11 shows the sensitivity of the Nusselt number to Rayleigh and Reynolds numbers during transition. As the Rayleigh number increases, the Nusselt number is only slightly affected. However, as a flow undergoes transition at a Reynolds number of 2,750, the Nusselt number increases dramatically. This is in contrast to buoyancy-affected flows, such as laminar flows, where the Nusselt number is significantly affected by changes in the

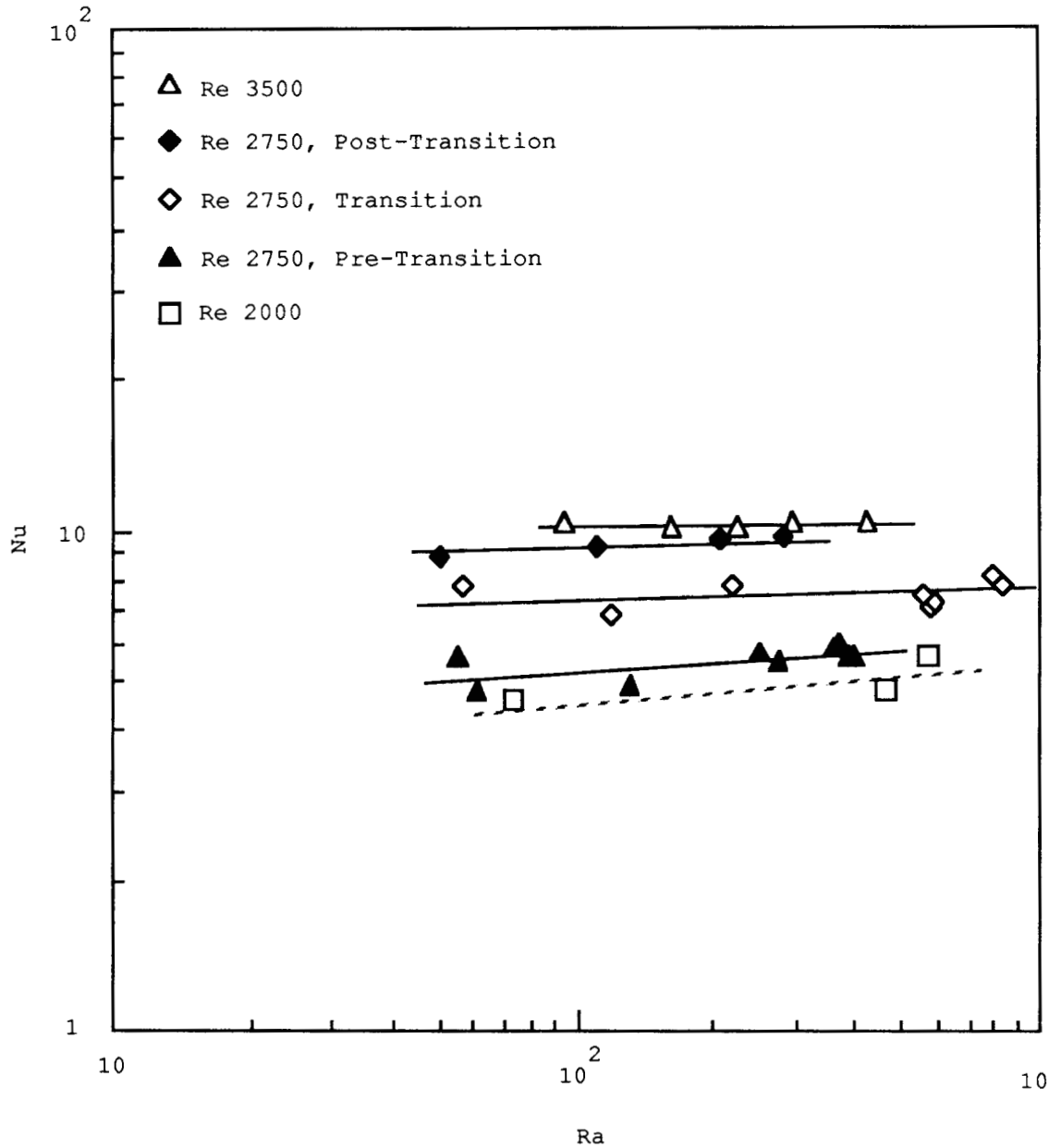

Figure 11. Plot of Nu vs. Ra

Rayleigh number. The characteristic slopes of these curves (Figure 11) suggest that, under the conditions investigated, the Reynolds number has a far more dominant effect on heat transfer than does the Rayleigh number.

Figure 12 relates the Nusselt number and Reynolds number for all data points. As can be seen from this figure, experimental data in the laminar range agree very well with the constant laminar Nusselt number for internal flows with constant heat flux (Nu = 4.36). Through transition, the Nusselt number increases, then levels off slightly as flow becomes turbulent. Disturbed laminar flows generally exhibited higher Nusselt numbers (or rates of heat transfer) than the conventional laminar flows experiencing constant wall heat flux. Turbulent flow Nusselt numbers were markedly lower than standard turbulent heat transfer correlations predict. Shown on Figure 12 is a heat transfer correlation presented by Sleicher and Rouse (22) for internal turbulent flow (horizontal tube) and experimental data from Schimdt (7) (horizontal tube flow with the top half of the tube heated). A comparison with these previous works shows that asymmetric wall heating in downflow tends to decrease the rate of heat transfer considerably, nearly a factor of two at a Reynolds number of 4,000.

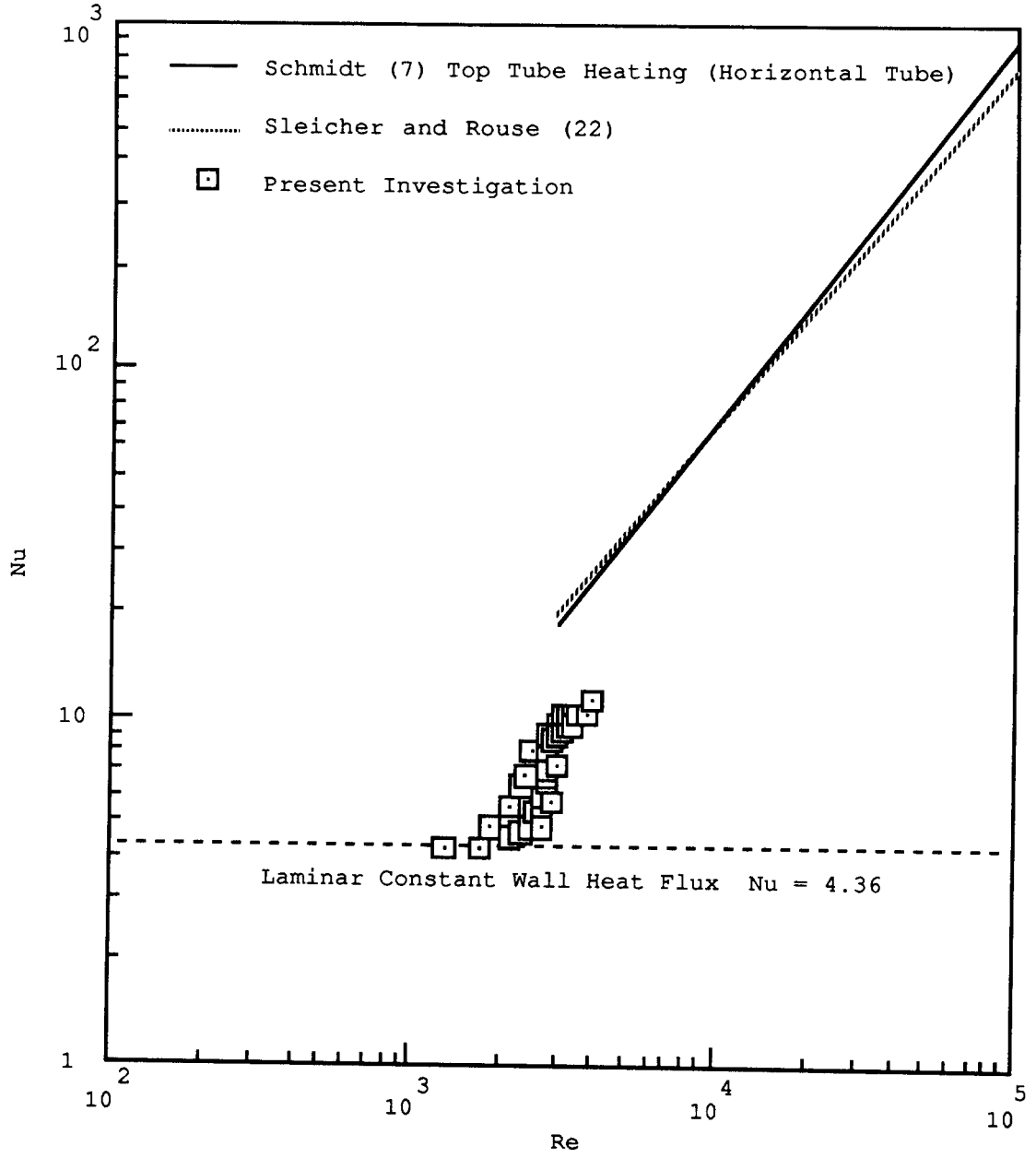

Figure 12. Plot of Nu vs. Re

CHAPTER 5

CONCLUSIONS AND RECOMMENDATIONS

Water flowing downward in a vertical tube is more unstable for the case of asymmetric wall heat flux than for the case of a uniform wall heat flux. However, it is still more stable than flow through a horizontal tube with uniform wall heat flux.

At low heating powers (and consequently small buoyant forces) heating had a clearly stabilizing effect on hydrodynamic transition. The critical Reynolds number increased from 2,400 to about 3,000 for the highest heating power tests.

As compared with the internal flow, constant flux heat transfer correlations, given in Schmidt (7) and Sleicher and Rouse (22), experimental data from the present investigation with asymmetric heat flux indicated noticeably lower rates of heat transfer. It is apparent that both tube orientation and symmetry of heating must be considered in the design process.

This author suggests the following recommendations for further study of this asymmetric heat flux boundary condition. If water is to be used as the heat transfer fluid it should be deaerated. In this investigation, as previously mentioned, small amounts of air were observed in the effluent during tests using higher heating powers. This could be eliminated by first deaerating the water. Another alternative would be to use an oil or glycol as the heat transfer fluid. This would have the added benefit of reducing the risk of obtaining local wall temperatures in excess of the fluid boiling temperature. Local boiling prohibited this investigation from studying the thermal turbulence region and may have influenced the observed thermal transition-like region.

Although this study has contributed to understanding the effect of asymmetric heating and tube orientation on flow stability and heat transfer, an exhaustive study is needed to investigate buoyancy-affected forced flow over a much broader range of Reynolds numbers. The addition of turbulent heat transfer data to the present investigation and the development of a turbulent heat transfer correlation would be very important in designing and evaluating solar central receivers.

REFERENCES

1.) R. W. Fox and A. T. McDonald, Introduction to Fluid Mechanics, 2nd ed., (John Wiley and Sons, 1978).

2.) M. A. El-Hawary, "Effect of Combined Free and Forced Convection on the Stability of Flow in a Horizontal Tube," Journal of Heat Transfer, 102:273-278, 1980.

3.) L. D. McCoy, "The Determination of Heat Transfer Coefficients in a Vertical Tube at Low Flows" (Master's thesis, Department of Mechanical Engineering, University of Louisville, 1972).

4.) T. M. Hallman, "Combined Forced and Free Convection in a Vertical Tube" (Ph.D. diss., Purdue University, 1958).

5.) G. F. Scheele, "The Effect of Natural Convection on Transition to Disturbed Flow in a Vertical Tube" (Ph.D. diss., Department of Chemical Engineering, University of Illinois, 1962).

6.) T. J. Hanratty, E. M. Rosen, and R. L. Kabel, "Effect of Heat Transfer on Flow Field at Low Reynolds Numbers in Vertical Tubes," Industrial & Engineering Chemistry, 50:815-820, 1958.

7.) R. Schmidt, "Experiments on Buoyancy-Affected and Buoyancy-Unaffected Turbulent Heat Transfer for Water in a Tube with Circumferentially Non-Uniform Heating" (Ph.D. diss., Department of Mechanical Engineering, University of Minnesota, 1977).

8.) A. W. Black and E. M. Sparrow, "Effects on Turbulent Heat Transfer in a Tube With Circumferentially Varying Thermal Boundary Conditions," Transactions of the ASME, 1967, pp. 258-268.

9.) A. R. Nagendra, "Interaction of Free and Forced Convection in Horizontal Tubes in the Transition Regime," Journal of Fluid Mechanics, 57(2): 269-288, 1973.

10.) E. K. Kalinin and S. A. Yarko, "Flow Pulsations and Heat Transfer in the Transition Region Between the Laminar and Turbulent Regimes in a Tube," International

Journal of Chemical Engineering, 6:571-574, 1966.

11.) H. Schlichting, Boundary Layer Theory, (6th ed.; New York McGraw-Hill, 1968), p.432.

12.) G. F. Scheele, E. M. Rosen and T. J. Hanratty, "Effect of Natural Convection on Transition to Turbulence in Vertical Pipes," Canadian Journal of Chemical Engineering, June 1960, pp. 67-73.

13.) G. F. Scheele and T. J. Hanratty, "Effect of Natural Convection Instabilities on Rates of Heat Transfer at Low Reynolds Numbers," AIChE J., 9(2): 183-185 , 1963.

14.) S. A. Guerrieri and R. J. Hanna, "Local Heat Flux in a Vertical Duct with Free Convection in Opposition to Forced Flow," ONR Final Report Contract N - ONR - 622(01), Nov. 1952.

15.) R. Siegel, E. M. Sparrow and T. M. Hallman, "Steady Laminar Heat Transfer in a Circular Tube with Prescribed Wall Heat Flux," Applied Scientific Research, 7(A): 386-392, 1958.

16.) W. C. Reynolds, "Heat Transfer to Fully Developed Laminar Flow in a Circular Tube with Arbitrary Circumferential Heat Flux," ASME Journal of Heat Transfer, 82:108-112, 1960.

17.) W. C. Reynolds, "Turbulent Heat Transfer in a Circular Tube with Variable Circumferential Heat Flux," International Journal of Heat and Mass Transfer, 6: 445-454, 1963.

18.) 3054A Data Acquisition System Library (9845B), Instruments Vol. 3A, Hewlett-Packard, Palo Altos, C.A., 94304.

19.) "Operating Instructions," Document number 74-691, Hy-Cal Engineering, Santa Fe Springs, C.A., 90670.

20.) Temperature Measurement Handbook 1985, p. T-39, Omega Engineering, Stamford, C.T., 06907.

21.) Personal Communication, Engineering Support, Rosemount, Minneapolis, M.N., 55435.

22.) C. A. Sleicher and M. W. Rouse, "A Convenient Correlation for Heat Transfer to Constant and Variable Property Fluids in Turbulent Pipe Flow," International Journal of Heat Mass Transfer, 18: 677-683, 1975.

23.) Application Note 290, "Practical Temperature Measurements," Hewlett-Packard, Palo Alto, C.A., 94304, 1983.

APPENDIX A

FLUID TEMPERATURE AND PRESSURE DROP FLUCTUATION OUTPUT

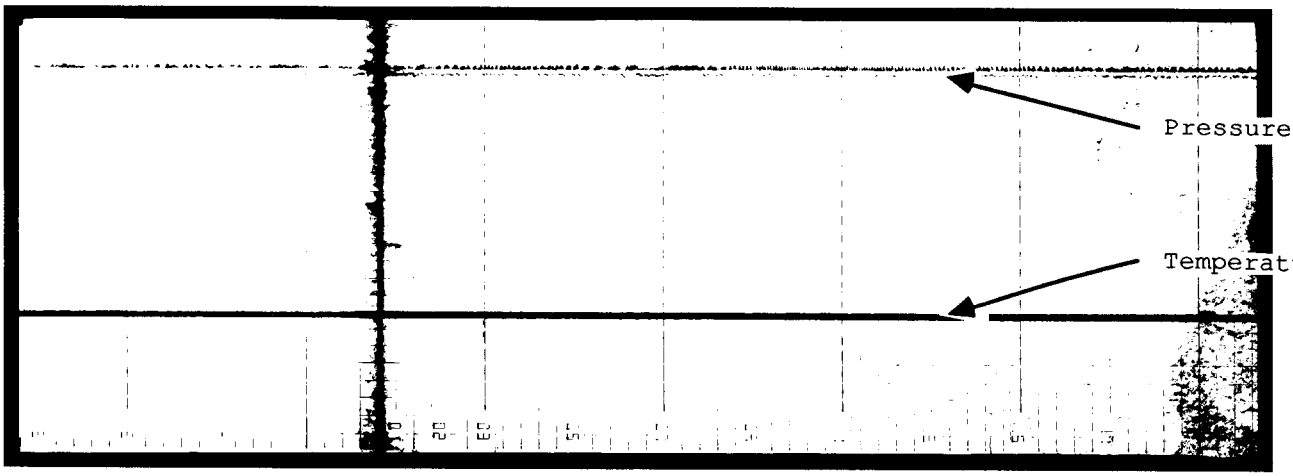

(a) Fluctuation Output, Test 1/3

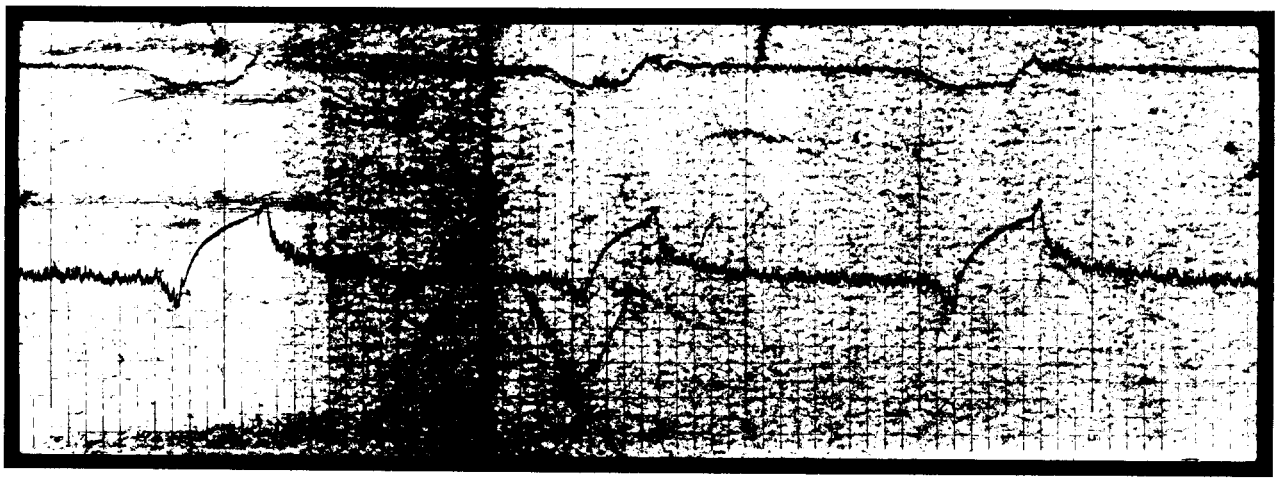

(b) Fluctuation Output, Test 5/2

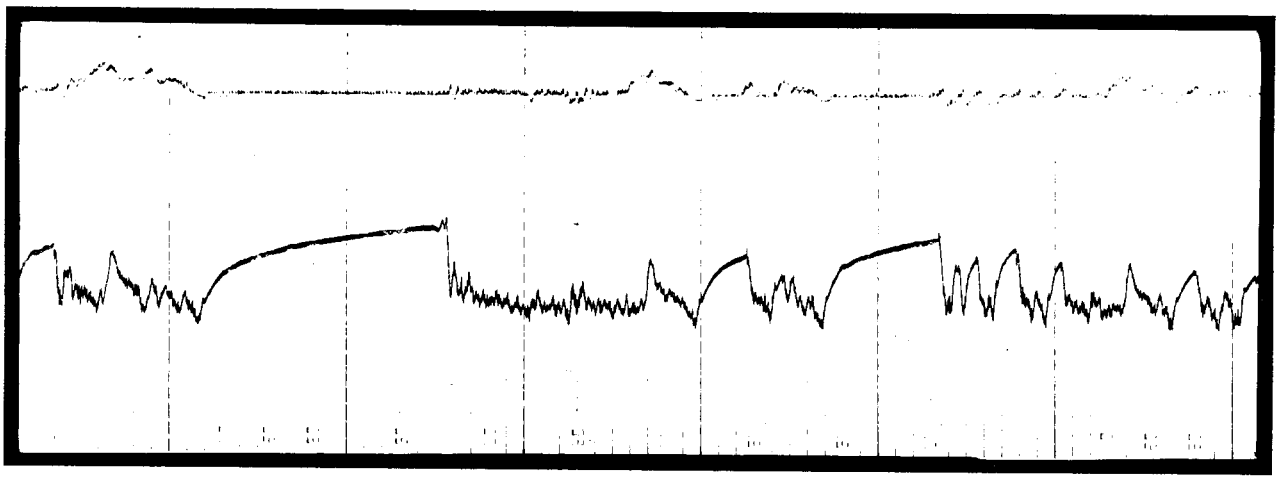

(c) Fluctuation Output, Test 7/1

Figure 13 (a), (b), (c). Constant Flowrate With Increasing Power

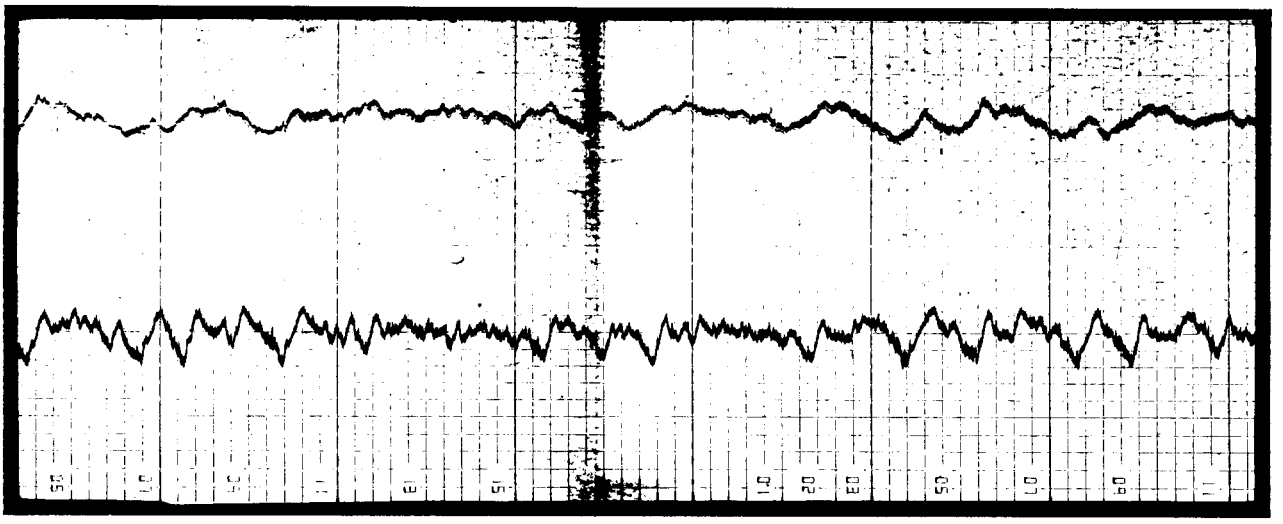

(d) Fluctuation Output, Test 7/2

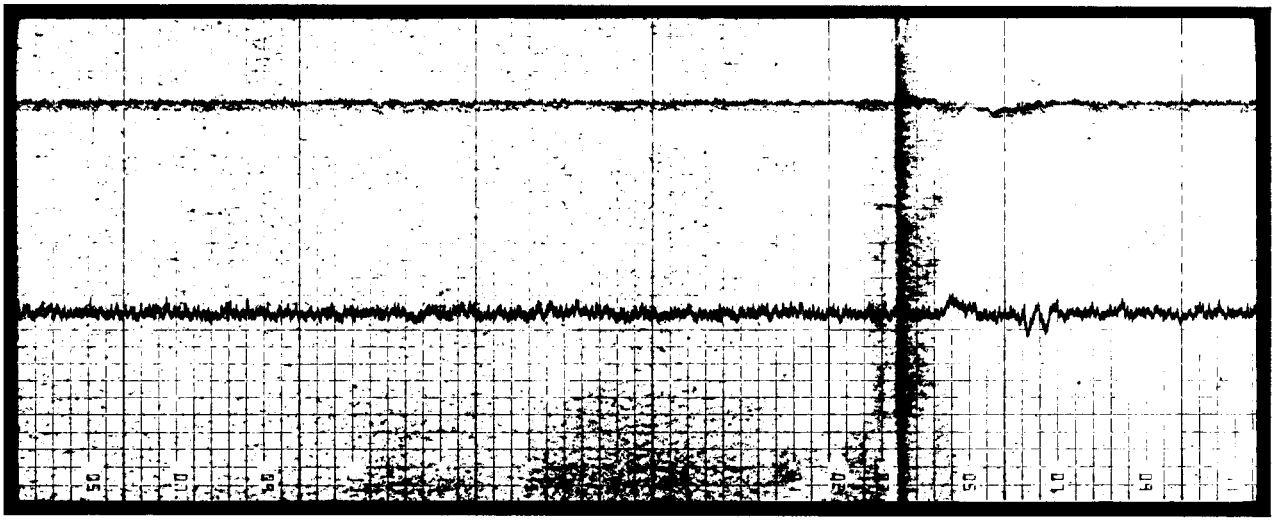

(e) Fluctuation Output, Test 7/3

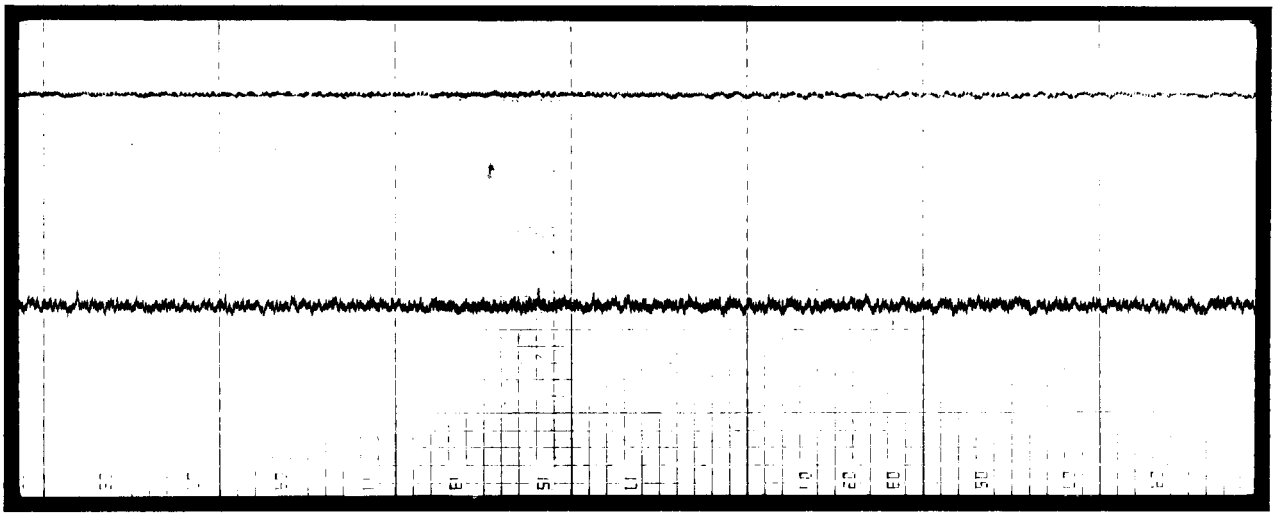

(f) Fluctuation Output, Test 7/4

Figure 13 (d), (e), (f). Constant Flowrate With Increasing Power (continued)

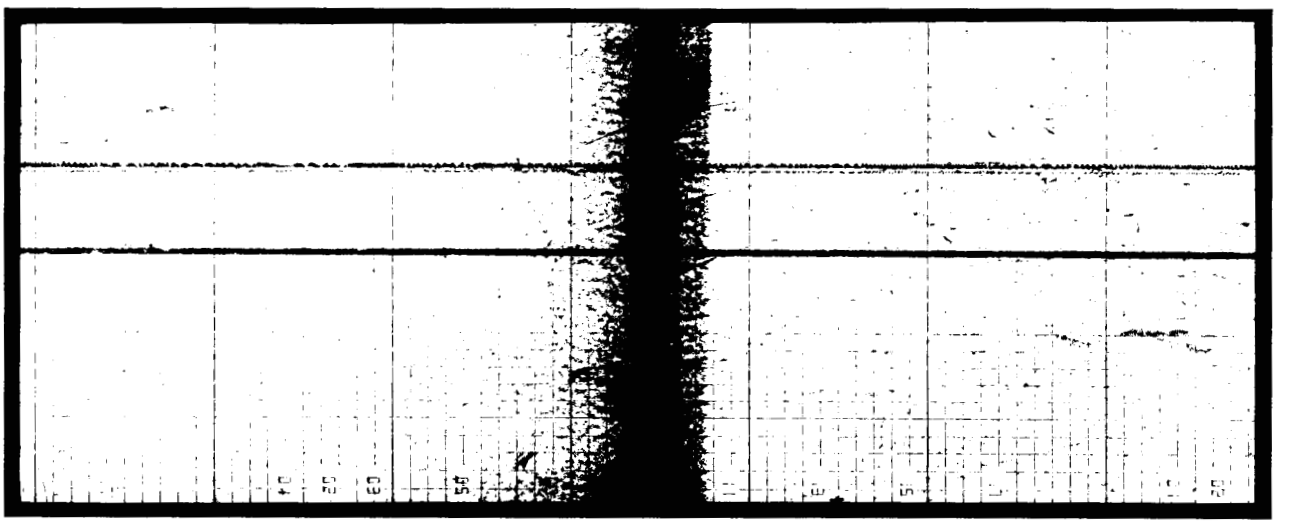

(a) Fluctuation Output, Test 3/1

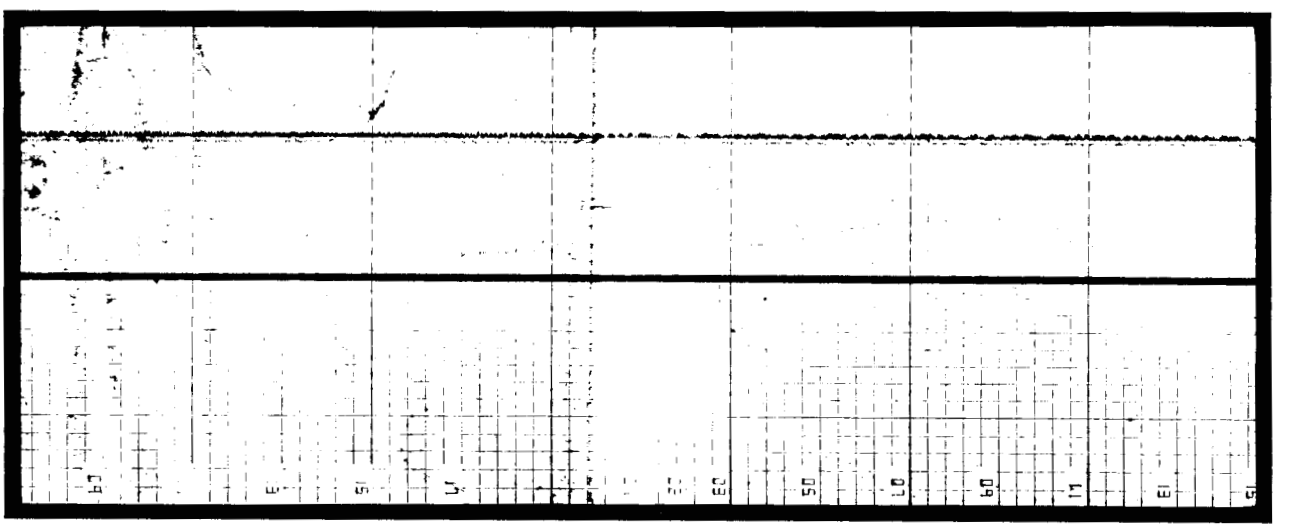

(b) Fluctuation Output, Test 3/2

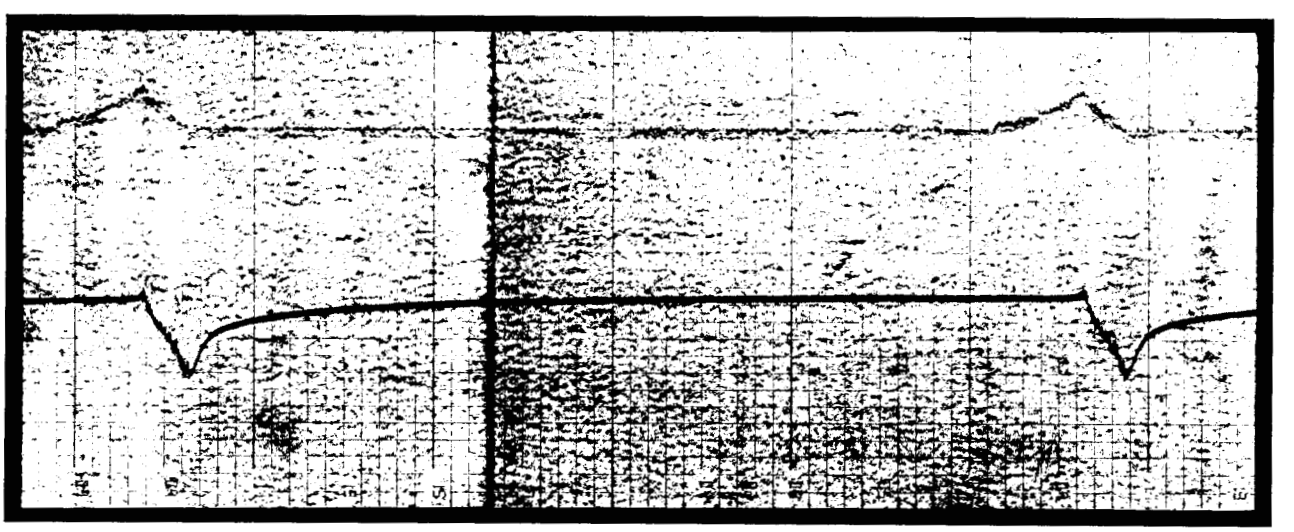

(c) Fluctuation Output, Test 3/3

Figure 14 (a), (b), (c). Constant Power With Increasing Flowrate

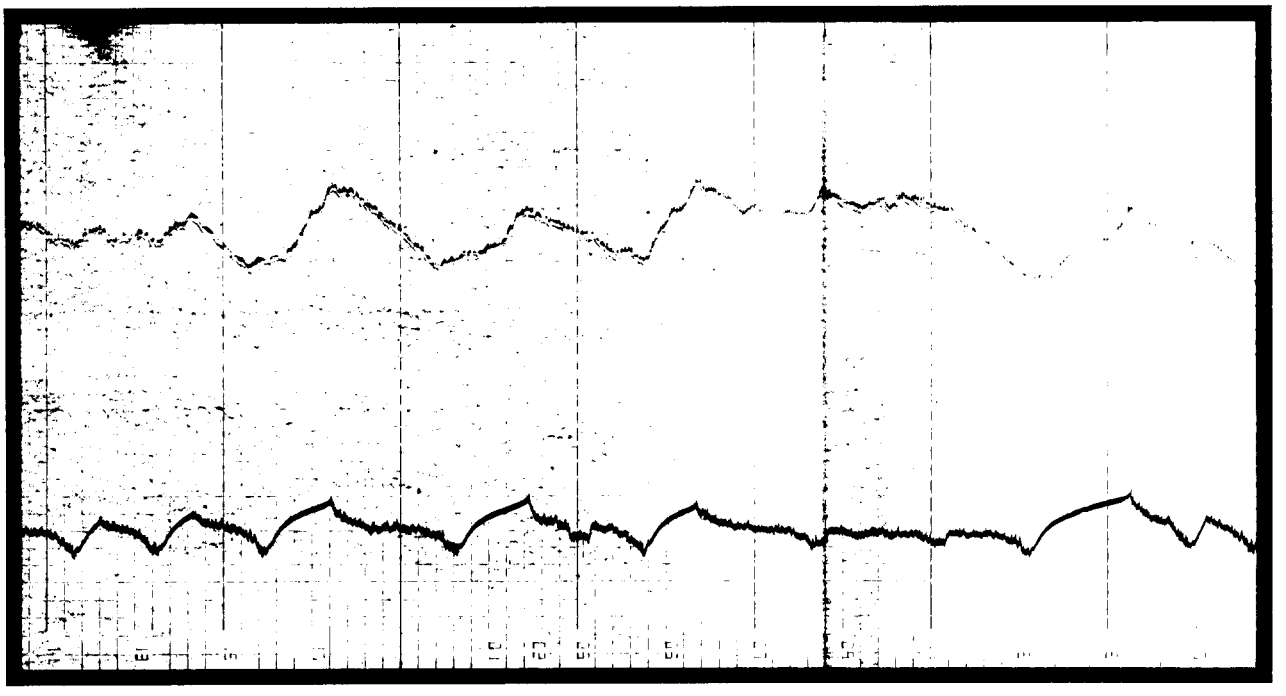

(d) Fluctuation Output, Test 3/4

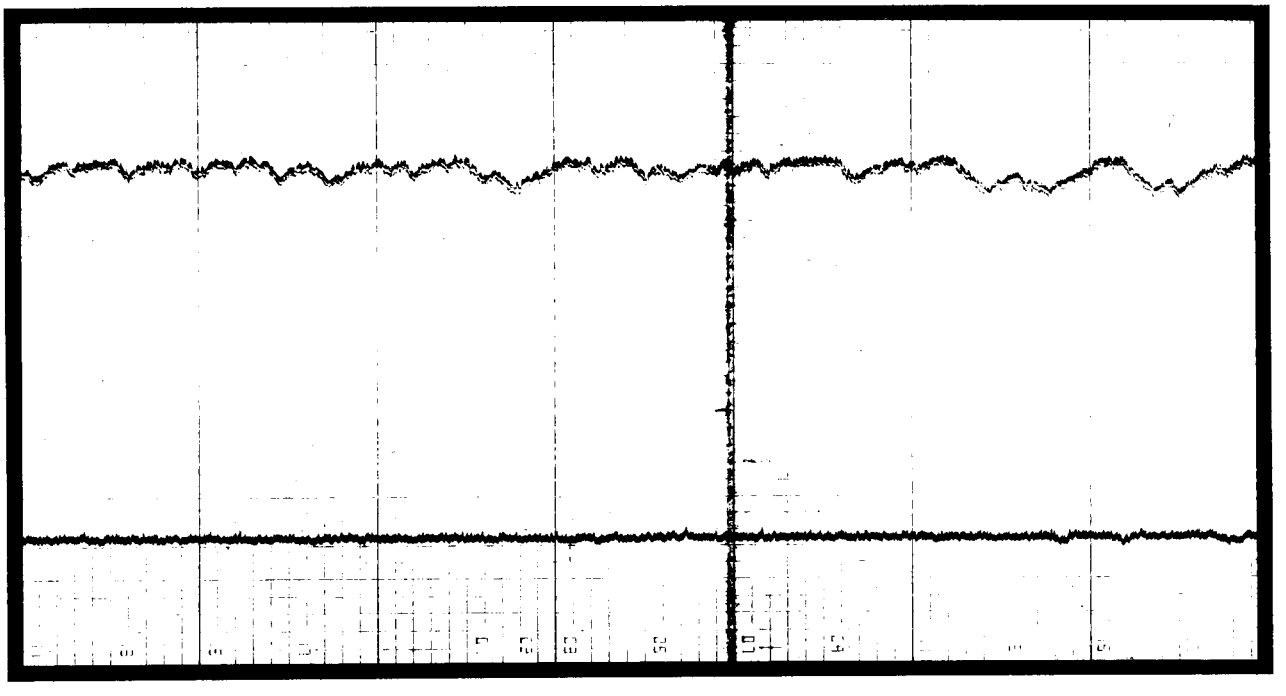

(e) Fluctuation Output, Test 3/5

Figure 14 (d), (e). Constant Power With Increasing Flowrate (continued)

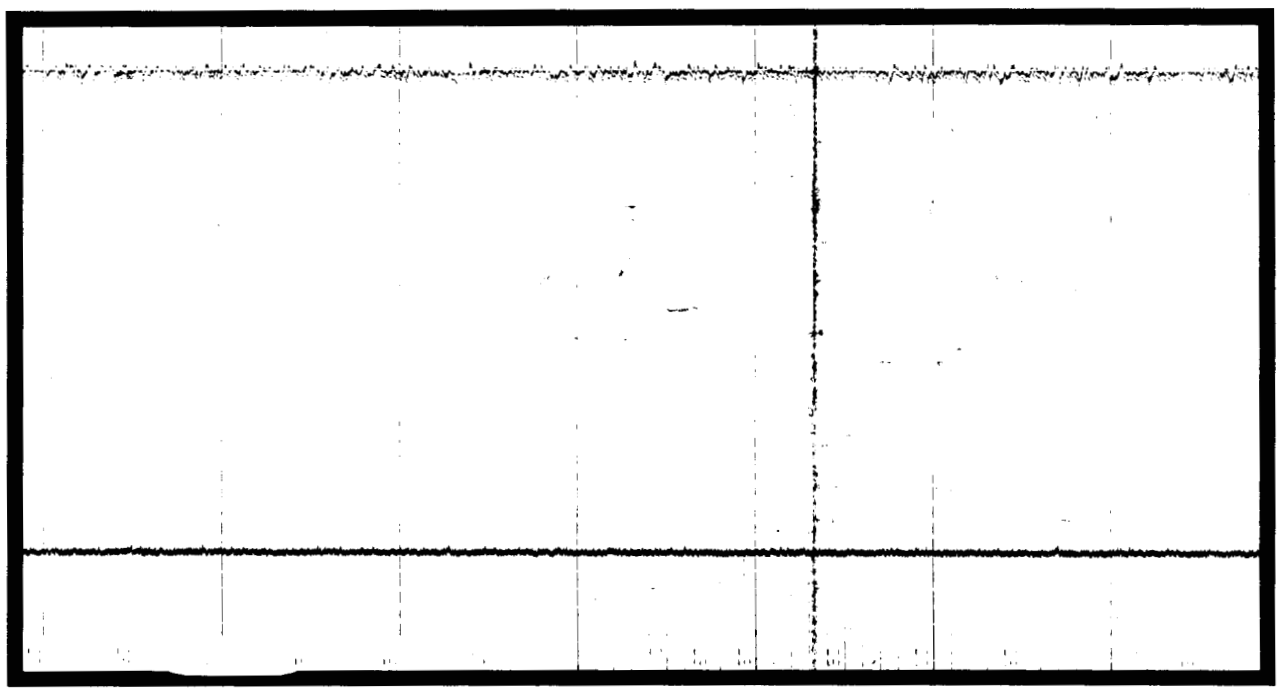

Figure 14 (f). Constant Power With Increasing Flowrate (continued)

APPENDIX B

ERROR ANALYSIS

An error analysis will now be presented to estimate the accuracy of the data. Because of the large number of variables involved in the calculations, it is impractical to perform an error analysis for each data point. Instead, four points 4/4, 6/4, 1/3, and 1/7 were choosen for analysis. Tests 4/4 and 6/4 represent average data points and reflect the magnitude of errors associated with the majority of the data. Tests 1/3 and 1/7 represent the lower and upper bounds for 15 percent of the data which had large errors.

Basic measured parameters, such as temperatures, tube diameter and tube length, were each assigned an uncertainty interval or a percent error interval based on calibration results and measuring techniques.

Inlet temperature, Ti (°C)	
-Reference error	±0.04 °C
-Difference between 36-gage thermocouples and reference	±0.04 °C
-Error in measuring head tank temperature	±0.10 °C
Total Error	±0.18 °C
Outlet temperature, To (°C)	
-Reference error	±0.04 °C
-Difference between 12-gage thermocouples and reference (20-50 °C range)	±0.08 °C
-Error in mixing cup measurement	±0.20 °C
Total Error	±0.32 °C
Wall temperature, Tw (°C)	
-Reference error	±0.04 °C
-Difference between 36-gage	

thermocouples and reference	
in the range 5-75 °C	±0.13 °C
Total Error	±0.17 °C

Inside tube diameter, Di (m)

-Error due to manufacturing tolerances	2.0%

Tube length, L (m)

-Error due to unheated length in test section caused by lower pressure tap	0.6%

Time, t (seconds)

-Error in time measurement	0.1 s

If two measurements were added or subtracted their individual errors were added such that the largest error was obtained.

Bulk fluid temperature rise, To-Ti (°C)

-Error in To	±0.32 °C
-Error in Ti	±0.18 °C
Total Error	±0.50 °C

Average bulk fluid temperature, Tb = (To+Ti)/2 (°C)

-Error in To	±0.32 °C
-Error in Ti	±0.18 °C
Total	±0.50 °C
Total Error ±0.50/2°C or	±0.25 °C

Difference between wall and average bulk fluid temperature, Tw-Tb (°C)

-Error in Tw	±0.17 °C
-Error in Tb	±0.25 °C
Total Error	±0.42 °C

Error estimates for fluid properties were calculated using Equation (A-1). Empirically derived equations for all fluid properties are in Appendix D and were evaluated at the average bulk fluid temperature.

$$\Delta y = \{ \Sigma [(dy/dx) \Delta x] \} \qquad \text{(A-1)}$$

eg., $\rho = 1001-0.0708*Tb-0.003609*Tb^2$

$d\rho/dTb = -0.0708-0.007218*Tb$

at $Tb = 20.3\ ^\circ C$ $d\rho/dTb = -0.2176$, $\Delta Tb = \pm 0.25\ ^\circ C$

therefore, $\Delta\rho = 0.0544$

The value for dy was then divided by y to give an error ratio or a percent error, $\Delta y/y$;

eg. $\Delta\rho = 0.0544$, $\rho = 998.1$, $\Delta\rho/\rho = 0.0001$

or 0.01 %

For dimensionless groups, which are a product of several parameters, Equation (A-2) was used along with the error ratios, $\Delta y/y$, for each of the parameters involved;

eg. if $y = (x^a * w^b) / z^c$,

$$\Delta y/y = [a^2 (\Delta x/x)^2 + b (\Delta w/w)^2 + c (\Delta z/z)^2]^{1/2}, \qquad \text{(A-2)}$$

$Re = (\rho * V * D) / \mu$,

$\Delta Re/Re = [(\Delta\rho/\rho)^2 + (\Delta V/V)^2 + (\Delta D/D)^2 + (\Delta\mu/\mu)^2]$.

Table 2 summarizes the percent errors involved for tests 4/4, 6/4, 1/3 and 1/7.

TABLE 2

Tests	4/4	6/4	1/3	1/7
	% error	% error	% error	% error
Ti	0.9	1.0	0.9	1.0
To	1.1	0.8	1.5	1.6

(Table 2 continued on next page)

TABLE 2 continued

Tb	1.0	0.9	1.2	1.3
To-Ti	5.0	2.5	19.5	25.8
Tw-Tb	2.0	1.1	4.7	9.4
Pr	0.6	0.6	0.6	0.6
m	5.7	5.7	5.7	5.7
q	7.6	6.2	20.3	26.4
f	6.5	6.6	6.9	6.4
Re	4.5	4.5	4.5	4.5
Ra	9.6	8.5	21.2	27.1
Gr	11.3	10.4	22.0	27.7
h	8.1	6.6	20.9	28.1
Nu	8.3	6.9	21.0	28.2

APPENDIX C

TABLE 3

LOCATION OF WALL THERMOCOUPLES (see Figure 5)

Thermocouple Number	Distance from inlet of test section (cm)	Distance in diameters	Location on circumference
1L	0.0	0	Left side
2R	7.0	9	Right
3L	13.9	18	Left
4R	20.1	26	Right
5T	27.1	35	Top
5R	27.1	35	Right
5L	27.1	35	Left
5B	27.1	35	Bottom
6R	41.1	53	Right
7L	54.2	70	Left
8R	68.2	88	Right
9L	82.1	106	Left
10T	109.2	141	Top
10R	109.2	141	Right
10L	109.2	141	Left
10B	109.2	141	Bottom
11R	136.3	176	Right
12L	150.3	194	Left
13R	163.5	211	Right
14L	177.4	229	Left
15T	191.4	247	Top
15R	191.4	247	Right
15L	191.4	247	Left
15B	191.4	247	Bottom
16R	197.5	255	Right
17L	204.5	264	Left
18R	211.5	273	Right
19L	218.5	282	Left

APPENDIX D

TABLE 4

TABULATED HEAT TRANSFER DATA

Test	Mass Flowrate x 10^3 (kg/s)	Bulk Fluid Temp. Tb (°C)	Outlet to Inlet Temp. To-Ti (°C)	Wall to Fluid Temp. Tw-Tb (°C)	Velocity (m/s)	Power (W)
1/1	8.08	21.6	5.2	10.0	0.1721	177
1/2	13.87	20.5	3.0	9.2	0.2953	175
1/3	16.48	20.3	2.6	8.9	0.3503	177
1/4	17.55	20.2	2.3	7.4	0.3733	172
1/5	18.24	20.0	2.4	5.7	0.3878	183
1/6	18.81	19.8	2.2	4.7	0.3985	172
1/7	20.31	19.6	1.9	4.5	0.4341	165
2/1	10.56	22.6	8.2	20.5	0.2245	361
2/2	14.75	21.6	6.1	19.1	0.3134	377
2/3	17.43	21.1	5.1	18.3	0.3700	374
2/4	18.25	20.9	4.8	13.1	0.3800	365
2/5	18.81	21.0	4.8	10.4	0.3988	376
2/6	19.43	20.9	4.5	9.5	0.4125	367
2/7	22.07	20.5	3.9	8.5	0.4694	360
3/1	10.66	25.7	14.1	31.2	0.2270	627
3/2	15.62	23.3	9.4	27.3	0.3322	617
3/3	17.67	23.0	8.8	27.1	0.3759	648
3/4	18.36	22.5	7.9	18.9	0.3905	605
3/5	19.06	22.3	7.6	15.3	0.4063	604
3/6	22.87	21.7	6.2	14.0	0.4866	589
4/1	11.95	26.8	16.0	34.2	0.2543	800
4/2	15.64	25.0	12.2	34.2	0.3339	801
4/3	17.30	24.7	11.5	34.1	0.3679	830
4/4	19.11	24.3	10.0	20.6	0.4064	803

4/5	19.72	23.7	9.8	18.6	0.4194	805
4/6	23.30	22.9	7.8	18.0	0.4955	756
5/1	12.82	29.0	19.6	36.7	0.2732	1,049
5/2	15.50	27.3	16.3	38.0	0.3301	1,060
5/3	17.02	26.8	15.4	36.5	0.3624	1,099
5/4	18.30	26.2	14.3	25.4	0.3895	1,096
5/5	19.64	25.4	12.9	24.5	0.4180	1,060
5/6	23.39	24.4	11.0	23.1	0.4975	1,077
6/1	18.25	23.4	9.6	18.3	0.3881	734
6/2	"	25.2	13.0	24.6	0.3883	993
6/3	"	26.7	15.9	29.9	0.3885	1,213
6/4	"	28.9	20.2	38.2	0.3887	1,538
7/1	16.12	24.7	11.7	31.7	0.3430	788
7/2	"	26.5	15.9	35.9	0.3431	1,072
7/3	"	28.8	20.2	40.2	0.3433	1,364
7/4	"	29.5	21.8	40.3	0.3434	1,467
8/1	14.90	24.4	12.5	33.5	0.3173	777
8/2	"	26.7	16.6	34.6	0.3172	1,036
8/3	"	29.0	21.1	40.1	0.3174	1,314
9/1	13.09	26.3	15.7	32.6	0.2795	861
9/2	"	27.9	18.8	36.0	0.2787	1,027
9/3	"	30.6	23.8	37.7	0.2789	1,303

APPENDIX E

TABLE 5

TABULATED DIMENSIONLESS GROUPS

(and heat transfer coefficient)

Test	f	Re	Ra	h ($W/m^2°C$)	Nu
1/1	0.0510	1277	137	332	4.28
1/2	0.0289	2138	73	358	4.62
1/3	0.0242	2525	61	372	4.80
1/4	0.0260	2679	55	433	5.58
1/5	0.0319	2776	50	606	7.82
1/6	0.0401	2839	50	684	8.84
1/7	0.0432	3073	43	697	9.01
2/1	0.0378	1702	227	330	4.24
2/2	0.0260	2321	159	370	4.76
2/3	0.0219	2713	129	384	4.94
2/4	0.0292	2834	119	524	6.74
2/5	0.0365	2914	119	677	8.72
2/6	0.0424	3008	112	728	9.38
2/7	0.0426	3398	94	799	10.31
3/1	0.0374	1845	471	378	4.81
3/2	0.0224	2558	275	425	5.45
3/3	0.0216	2872	249	449	5.76
3/4	0.0320	2951	217	601	7.71
3/5	0.0401	3059	206	741	9.52
3/6	0.0409	3612	161	790	10.15
4/1	0.0307	2118	568	439	5.58
4/2	0.0234	2663	394	441	5.63
4/3	0.0218	2922	362	459	5.85
4/4	0.0360	3202	319	734	9.37
4/5	0.0397	3261	292	813	10.40

4/6	0.0390	3782	220	791	10.13
5/1	0.0327	2394	778	538	6.80
5/2	0.0234	2786	599	524	6.65
5/3	0.0224	3023	550	567	7.19
5/4	0.0362	3203	494	812	10.32
5/5	0.0400	3374	425	813	10.36
5/6	0.0381	3929	343	878	11.21
6/1	0.0341	2995	282	756	9.67
6/2	0.0365	3120	424	761	9.69
6/3	0.0371	3228	564	765	9.72
6/4	0.0312	3402	800	758	9.57
7/1	0.0209	2726	370	467	5.97
7/2	0.0268	2865	564	561	7.13
7/3	0.0312	2938	799	638	8.07
7/4	0.0337	3045	888	685	8.64
8/1	0.0254	2506	388	436	5.57
8/2	0.0296	2637	588	564	7.16
8/3	0.0342	2783	839	616	7.79
9/1	0.0297	2297	546	497	6.32
9/2	0.0332	2387	709	536	6.79
9/3	0.0378	2541	1027	650	8.18

DISTRIBUTION:

Advanced Thermal Systems
5031 W. Red Rock Drive
Larkspur, CO 80118
attn: D. Gorman

Aerospace Corporation
Energy Systems Group
PO Box 92957
Los Angeles, CA 90009
attn: P. Munjal

Analysis Review and Critique
6503 81st St.
Cabin John, MD 20818
attn: C. LaPorta

Arizona Public Service Company (3)
PO Box 21666
Phoenix, AZ 85036
attn: E. Weber
J. McGuirk
D. Thornburg

Babcock and Wilcox (4)
91 Stirling Ave.
Barberton, OH 44203
attn: D. Young
D. Smith
P. Reed
C. Dalton

Battelle Pacific Northwest Laboratory
PO Box 999
Richland, WA 99352
attn: T.A. Williams

Bechtel National, Inc.
50 Beale Street
50/15 D8
San Francisco, CA 94106
attn: P. DeLaquil

Black and Veatch Consulting Engineers (3)
PO Box 8405
Kansas City, MO 64114
attn: J. C. Grosskreutz
J. E. Harder
L. Stoddard

Boeing Aerospace
Mail Stop JA-83
Huntsville, AL 35807
attn: W. D. Beverly

Tom Brumleve
1512 N. Gate Road
Walnut Creek, CA 94598

California Energy Commission
1516 Ninth Street, Mail Stop 43
Sacramento, CA 95814
attn: A. Jenkins

California Public Utilities Commission
Resource Branch, Room 5198
455 Golden Gate Avenue
San Francisco, CA 94102
attn: T. Thompson

Centro Investigations Energetica
Medroansental Technologie (CIEMAT)
Avda. Complutense 22
28040 Madrid
SPAIN
attn: F. Sanchez

DFVLR EN-TT (2)
Institute for Technical Thermodynamics
Pfaffenwaldring 38-40
7000 Stuttgart 80
FEDERAL REPUBLIC OF GERMANY
attn: Dr. M. Becker
Dr. C. Winter

El Paso Electric Company
PO Box 982
El Paso, TX 79946
attn: J. E. Brown

Electric Power Research Institute (2)
PO Box 10412
Palo Alto, CA 94303
attn: J. Bigger
E. DeMeo

Foster Wheeler Solar Development Corp.
12 Peach Tree Hill Road
Livingston, NJ 07039
attn: S. F. Wu

Georgia Institute of Technology
GTRI/EMSL Solar Site
Atlanta, GA 30332

IA/SSPS Project
Apartado 649
Almeria
SPAIN
attn: C. Arano

Jet Propulsion Laboratory
4800 Oak Grove Drive
Pasadena, CA 91103
attn: M. Alper

Los Angeles Dept. of Water and Power
Alternate Energy Systems
Room 661A
111 North Hope Street
Los Angeles, CA 90012
attn: Hung Ben Chu

Tom Tracey
6922 South Adams Way
Littleton, CO 80122

McDonnell Douglas (2)
MS 49-2
5301 Bolsa Avenue
Huntington Beach, CA 92647
attn: R. L. Gervais
J. E. Raetz

Meridian Corporation
5113 Leesburg Pike
Falls Church, VA 22041
attn: D. Kumar

Public Service Company of New Mexico
M/S 0160
Alvarado Square
Albuquerque, NM 87158
attn: T. Ussery
A. Martinez

Pacific Gas and Electric Company (2)
3400 Crow Canyon Road
San Ramon, CA 94526
attn: G. Braun
T. Hillesland

Polydyne, Inc.
1900 S. Norfolk Street, Suite 209
San Mateo, CA 94403
attn: P. Bos

Public Service Company of Colorado
System Planning
5909 E 38th Avenue
Denver, CO 80207
attn: D. Smith

Rockwell International
Rocketdyne Division
6633 Canoga Avenue
Canoga Park, CA 91304
attn: J. Friefeld

San Diego Gas and Electric Company
PO Box 1831
San Diego, CA 92112
attn: R. Figueroa

Sandia Solar One Office
PO Box 366
Daggett, CA 92327
attn: A. Snedeker

Science Applications International Corp.
10401 Roselle Street
San Diego, CA 92121
attn: B. Butler

Solar Energy Research Institute (5)
1617 Cole Boulevard
Golden, Co 80401
attn: B. Gupta
L.M. Murphy
J. Andersonh
M. Carasso

Solar Kinetics, Inc.
PO Box 47045
Dallas, TX 75247
attn: J. A. Hutchison

Solar Power Engineering Company (2)
PO Box 91
Morrison, CO 80465
attn: H. C. Wroton
T. Buna

Southern California Edison
PO Box 325
Daggett, CA 92327
attn: C. Lopez

Stearns Catalytic Corporation
PO Box 5888
Denver, CO 80217
attn: T. E. Olson

Stone and Webster Engineering Corp.
PO Box 1214
Boston, MA 02107
attn: R. W. Kuhr

U.S. Department of Energy (5)
Forrestal Building
Code CE-314
1000 Independence Ave SW
Washington, DC 20585
attn: H. Coleman
S. Gronich
F. Morse
M. Scheve
H. Shivers

U. S. Department of Energy
Forrstal Building
Code CE-33
1000 Independence Avenue SW
Washingotn, DC 20585
attn: C. Carwile

U. S. Department of Energy
Albuquerque Operations Office
PO Box 5400
Albuquerque, NM 87115
attn: D. Graves

U. S. Department of Energy
San Francisco Operations Office
f1333 Broadway
Oakland, CA 94612
attn: R. Hughey

University of Houston (2)
Solar Energy Laboratory
4800 Calhoun
Houston, TX 77704
attn: A. F. Hildebrandt
L. Vant-Hull

6000 D. L. Hartley
6200 V. L. Dugan
6220 D. G. Schueler
6220 A. V. Poore
6222 J. V. Otts (4)
6226 J. M. Chavez
6226 C. E. Tyner
6226 J. W. Grossman
6226 J. T. Holmes (20)
8100 E. E. Ives
8130 J. D. Gibson
8133 A. C. Skinrood
8133 L. G. Radosevich
3141 S. A. Landenberger (5)
3154-3 C. H. Dalin (28) DOE/OSTI
3151 W. L. Garner (3)
8024 P. W. Dean